# Refining Metallurgical Grade Silicon by Chlorination Treatment with Emphasis on Aluminum Removal

# Refining Metallurgical Grade Silicon by Chlorination Treatment with Emphasis on Aluminum Removal

**By Mahboob Bolandi, M. E. Sc., B. E. Sc.**

A Thesis Submitted to the School of Graduate Studies in Partial Fulfillment of the Requirements for the Degree Master of Applied Science

Master of Applied Science (2012) McMaster University

(Materials Science and Engineering) Hamilton, Ontario

TITLE: Refining Metallurgical Grade Silicon by Chlorination Treatment with Emphasis on Aluminum Removal

AUTHOR: Mahboob Bolandi, M.E.Sc. (Sharif University of Technology), B.E.Sc. (Tabriz University)

SUPERVISOR: Prof. Antony Petric

CO-SUPERVISOR: Prof. Kenneth Coley

NUMBER OF PAGES: x, 103

## Abstract

A supply shortage of solar-grade silicon in recent years resulted from a rapid expansion of the solar cell industry. Therefore, many efforts have been done to obtain reliable metallurgical methods for production of SoG silicon from metallurgical grade silicon.

In this research, refining of metallurgical grade silicon by chlorination treatment with the emphasis on Al removal was investigated. Thermodynamic calculations through Factsage confirmed the feasibility of Al removal in repeated steps of chlorination. Therefore, an Ar+$SiCl_4$ gas mixture with different flow rates was applied to the silicon melt by blowing and injection methods at different temperatures and the ICP-OES was used for analysis of the impurities in silicon.

Results revealed that Al removal from silicon by chlorination treatment under the conditions employed in this study is first order reaction with respect to Al. By increasing the temperature in the chlorination process, the rate constant increases which is related to an increase in the liquid mass transfer rate. Also the observed higher rates of Al removal under injection conditions appear to be the result of improved stirring in the melt rather than an increase in the interfacial area.

## Acknowledgement

I would like to express my sincere gratitude to my supervisors, Prof. Antony Petric and Prof. Kenneth Coley. They supported me and provided valuable advice, encouragement and lots of good ideas. I am very proud to have worked under their supervision and benefited from their knowledge and experience.

I also would like to record my sincere thanks to my former supervisory committee member, Dr. Mani Subramanian for his valuable cooperation and help during my period of study.

I extend my sincere thanks to the technical staffs in the department of Materials Science and Engineering, Ed McCaffery, Doug Culley, as well as Jim Garrett for their skillful assistance during my experimental work.

I am also greatly indebted to Diana Maltese, Nanci Cole and Jane Mah for being kind friends, and for their assistance with administrative matters.

I wish to thank 6N Silicon Company for providing the MG silicon for this research and McMaster University for financial supports.

My profound love and appreciation go to all members of my family for their love and support. To my family I dedicate this thesis.

# Table of Contents

## Table of Figures

## Table of Tables:

# 1. Introduction

Solar cell production has increased significantly due to a growing desire to reduce reliance on fossil fuels with their negative consequences on the environment. Worldwide production of photovoltaic modules is estimated to approach 18 GW annually by 2020 from a production level of 278 MW in 2000. [1] Materials resources for this application are dependent on expensive, off-spec semiconductor-grade silicon (SEG-Si). A supply shortage of solar-grade silicon (SoG-Si) in the early 2000s resulted from a rapid expansion of the solar cell industry. Since considerable part of the total cost is related to fabrication of the silicon for solar cell, development of a low-cost silicon refining process is essential for the widespread use of solar cells.

Most of the research on silicon production begins with the use of metallurgical-grade silicon (MG-Si) as the feedstock. [2-8] Some of the most common refining techniques currently being used are directional solidification, vacuum treatment of the melt to lower volatile elements, chemical reaction to form volatile species of impurities, oxidation to form separate oxide phases, and slag treatment of impurities. Removal of impurities from a silicon melt first requires a reaction, such as oxidation, to form an impurity species, and then partitioning of the species from molten silicon into another phase. In theory, multiple simple purification procedures to upgrade molten MG silicon plus directional solidification is the solution to the problem. The most favorable technique to produce SoG silicon is by removing impurities, such as boron, aluminum

and phosphorus in the molten metallurgical grade silicon (MG Si) followed by directional solidification.

## 2. Literature review

Early silicon refining methods were based on the fact that during solidification, the last liquid to solidify contains most of the impurities. Zone refining was the first silicon purification technique which was widely used industrially. In this technique, small length of MG-Si rod is heated to melt at one end then, the molten region is slowly transferred along the rod while the silicon cools and re-solidifies behind the moving molten region. Since most impurity elements tend to stay in the molten zone rather than re-solidify, after finishing the process, most of the impurities in the rod will be transferred into the end which solidified last. The end part containing high concentration of impurities is cut off and the process is repeated if a higher purity is needed.

In the well known Siemens process, high purity silicon rods are exposed to trichlorosilane gas at 1150°C. According to Eq. 1, the trichlorosilane gas ($HSiCl_3$) decomposes and deposits extra silicon onto the rods, enlarging them.

$$2\ HSiCl_3 \rightarrow Si + 2\ HCl + SiCl_4 \qquad \text{Eq.1}$$

SoG-Si can be manufactured either by simplification or modification [9-12] of the standard Siemens technique based on distillation of gaseous compounds containing mostly silicon, or by purification of MG silicon to lower concentrations of P, B, Al, O, C,

and transition metals. The refining processes that are most frequently stated in the literature consist of one of the following techniques or combination of them;

## 2.1. Acid leaching

In this method, MG-Si is crushed into powder with 70 micron particle size or less, and then treating this powder with various acids (e.g., aqua regia, hydrochloric acid, hydrofluoric acid) to dissolve metal clusters, frequently found in MG-Si at grain boundaries which are exposed during powdering [13]. It is possible to get silicon with a purity of 99.9–99.97% [14-16]. The disadvantage of this technique is that it is not effective in removing impurities dissolved intragranularly in high concentrations, e.g., B and P.

## 2.2. Directional solidification

During crystal pulling from the melt (e.g., Czochralski or float zone growth) or directional solidification of the molten silicon (e.g., float zone Si) impurities segregate to the melt [9,17-18]. At the end of the growth run, the majority of impurities is found in a thin layer near the top of the directionally solidified ingot. Such purification runs can be used to improve the purity of MG-Si. The efficiency of removal of impurities from silicon depends on their segregation coefficients. Except for B and P, most impurities have a segregation coefficient of $10^{-3}$ or less; for example, for Al it is 0.0028. The segregation

coefficients of B and P are 0.8 and 0.35, respectively. Therefore, most impurities except B and P can be removed by directional solidification. Several approaches to produce SoG silicon feedstock have been pursued, but none of these processes are commercialized because they could not economically remove B and P from MG silicon. A comparison of typical impurities in MG silicon and SoG silicon is shown in table 1.

Table 1: A comparison of typical impurities in MG silicon and SoG silicon [13]

| Impurity Elements | Impurity Content (ppmw) | | |
|---|---|---|---|
| | MG Silicon | | SoG Silicon |
| | 98-99% | 99.5% | |
| Al | 1000-4000 | 50-600 | <0.1 |
| Fe | 1500-6000 | 100-1200 | <0.1 |
| Ca | 250-2200 | 100-300 | <1 |
| Mg | 100-400 | 50-70 | <1 |
| Mn | 100-400 | 50-100 | <<1 |
| Cr | 30-300 | 20-50 | <<1 |
| Ti | 30-300 | 10-50 | <<1 |
| Cu | 20-40 | <10 | <1 |
| B | 10-50 | 10-15 | 1-1.5 |
| P | 20-40 | 10-20 | 0.1-1 |

The change in impurity content by solidification refining together with the required impurity limit for SoG-Si is shown in Figure 1. Most impurities, except for phosphorus, boron, oxygen and carbon, can be eliminated to the required concentration by applying solidification refining twice.

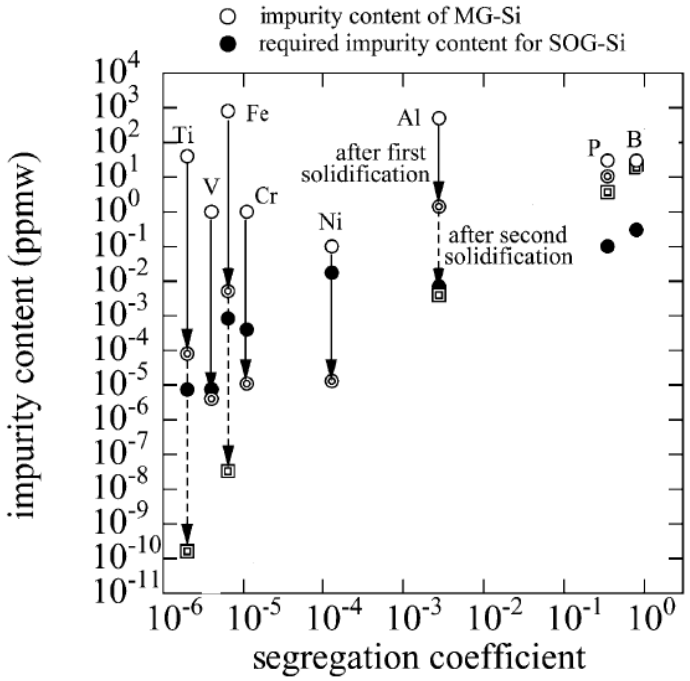


Figure 1: Change of impurity content by solidification refining [19]

## 2.3. Melting and refining of silicon with a reactive plasma

A plasma torch is used to melt the near-surface layer of silicon. In this technique, inert and reactive gases are usually being used; argon as an inert gas promotes the refining

process through stirring. Reactive gases such as hydrogen, oxygen, and water vapor react with impurities in the melt and form volatile compounds [20-27].

## 2.4. Vacuum processing

The simplest refining step is to remove volatile elements from MG silicon to the vapor; heating MG silicon in a molten stage under vacuum can enhance this. Vapor pressure of silicon at 1427ºC, a little above the melting point, is 0.0689 Pa and therefore, pure elements that have higher vapor pressure than silicon at 1427ºC can be expected to be removed. A major advantage of this refining step is that the impurities are removed irreversibly from the MG silicon. Vacuum processing of molten silicon has been shown to be most effective for reducing P concentration in silicon. [28-29]

## 2.5. Formation of volatile species

When the impurities can be reacted to form volatile molecular species, impurity elements can be eliminated through evaporation by injecting chlorine, oxygen, wet hydrogen, $SiCl_4$, $CO_2$, or their combinations. Reaction of these gases with impurity elements in liquid silicon and formation of volatile species that evaporate from the liquid, results in considerable removal. For instance, chloride of most metals and BOH are volatile. This technique is good for removal of Al, Ca, C, Mg, Fe, B, P, and Ti.

Table 2: Volatilization refining methods for removing impurities from liquid MG Si [31]

| Atomic # | El. | Volatilization (Liquid to Vapor) | |
|---|---|---|---|
| | | Elemental | Complexed Vapor Species* |
| 3 | Li | High | LiCl(g) |
| 5 | B | V. Low | HBO |
| 9 | F | High | NaF |
| 11 | Na | High | NaCl |
| 12 | Mg | High | $MGCl_2$ |
| 13 | Al | Moderate | AlCl, $AlCl_3$ |
| 14 | Si | | $SiCl_2$, SiO |
| 15 | P | Moderate | $P_2$, also $PH_2$, (PH, $PH_3$) or PO |
| 16 | S | High | SiS, $H_2S$, HS, $SiS_2$, $S_2$ |
| 17 | Cl | High | (NaCl) |
| 19 | K | High | KCl |
| 20 | Ca | High | $CaCl_2$ |
| 21 | Sc | Low | $ScCl_2$ |
| 22 | Ti | V Low | $TiCl_2$, $TiCl_3$ |
| 23 | V | V. Low | |
| 24 | Cr | Low | |
| 25 | Mn | high | |
| 26 | Fe | V. Low | $FeCl_2$ |
| 27 | Co | V. Low | $CoCl_2$ |
| 28 | Ni | V. Low | $NiCl_2$ |
| 29 | Cu | Moderate | CuCl |
| 30 | Zn | V. High | ($ZnCl_2$) |
| 31 | Ga | High | |
| 32 | Ge | Low | |
| 33 | As | High | |
| 34 | Se | V. High | |
| 37 | Rb | V. High | RbCl |
| 38 | Sr | V. High | $SrCl_2$ |
| 39 | Y | V. Low | |
| 40 | Zr | V. V. Low | |
| 41 | Nb | V. Low | |
| 42 | Mo | V. V. Low | |
| 47 | Ag | High | |
| 48 | Cd | High | |

*Calculated for 1 bar pressure, injected gas consisting of 45% Ar, 45% HCl and 10% $H_2O$.

Volatile compounds of impurity elements can be formed by reacting solid powders or gases. This can be done by addition of these powders either to the initial charge of MG-Si before melting or during the process. A list of the volatile species can be seen in table 2. [30-31]

### 2.5.1. Chlorination process

This technique is based on the reactivity of impurities in molten MG silicon toward halogens such as Cl or hydrogen halides to form volatile halides. The Gibbs energy of formation of the halides of silicon and the major impurities in MG silicon at 1427°C is summarized in table 3. Since all the chlorides have negative and relatively large Gibbs energies of formation and are volatile at the melting point of silicon, the treatment of molten MG silicon with chlorine should result in considerable purification. [30]

Table 3: Gibbs Energy of Formation of some chlorides [30]

| Chlorides | Gibbs Energy of Formation (kJ/mole $Cl_2$) at 1427°C |
|---|---|
| $AlCl_3$ | -324 |
| $BCl_3$ | -211 |
| $FeCl_2$ | -206 |
| $FeCl_3$ | -142 |
| $SiCl_4$ | -218 |

Chlorination treatment could be more effective in removing Al than other elements since $AlCl_3$ is more stable than silicon chlorides. In the experimental procedure, the activity or partial pressure will determine if the process is appropriate for silicon refinement. By using $SiCl_4$ as an example, the following reaction is expected to happen;

$$SiCl_4 + 4/3\ Al\ (in\ the\ melt) = 4/3\ AlCl_3 + Si \qquad \text{Eq. 2}$$

Since Al is chemically more reactive than silicon, chemical treatment of the melt is effective for the preferential removal of Al from MG silicon. Chu et al [30] reported that Al content could be reduced from 1000 ppmw to less than 50 ppmw by using silicon tetrachloride. Furthermore, combination of this method with unidirectional solidification could decrease Al level down to about 10 ppmw.

### 2.5.2. Refining by Oxygen

Gas injection and volatilization of compounds was the very first refining method for boron removal from liquid silicon. Theuerer [32] reported that during zone refining of silicon, by injecting water vapor under protective $H_2$, the electrical resistivity of silicon was increased significantly, which was attributed to volatilization of boron-containing species from silicon melt. More recently, Wu et al [33] reported boron removal by oxygen and oxygen water vapor. In their attempt, the impurity element boron dissolved in liquid silicon, [B], was oxidized into gaseous boron oxide species ($B_xO_y$) by oxygen.

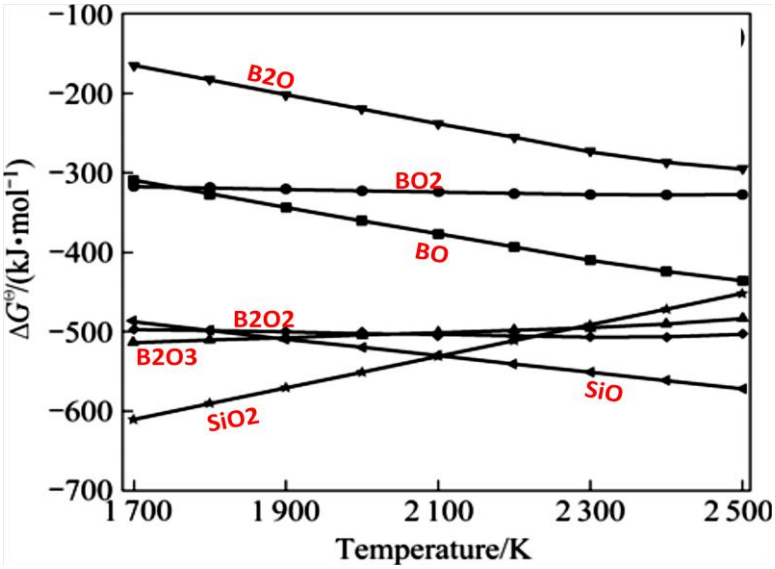


Figure 2: Gibbs free energy change vs temperature for oxidation reactions per mole of $O_2$ [33]

Based on NIST-JANAF Thermochemical Tables, calculations of the relationship between Gibbs free energy change of oxides ($B_xO_y$, $SiO_2$, SiO) and temperature is shown in Figure 2. According to the diagram, the most stable products are in the order of $B_2O_3$, $B_2O_2$, BO, $BO_2$ and $B_2O$ at 1700 K. Also according to the diagram, the Gibbs free energy of formation of $SiO_2$ and SiO are more negative in the temperature range of 1685-2100 K and 2100-2500 K, respectively. Therefore at 1600-2500 K, boron in MG silicon will not be removed by oxidization into $B_xO_y$ products and only silicon is oxidized to $SiO_2$ and SiO.

Under limited temperature and pressure conditions, $SiO_2$ will react to [B] to form gaseous boron oxides ($B_xO_y$). The relationship between the Gibbs free energy and temperature for the reactions between $SiO_2$ and [B] is depicted in Figure 3.

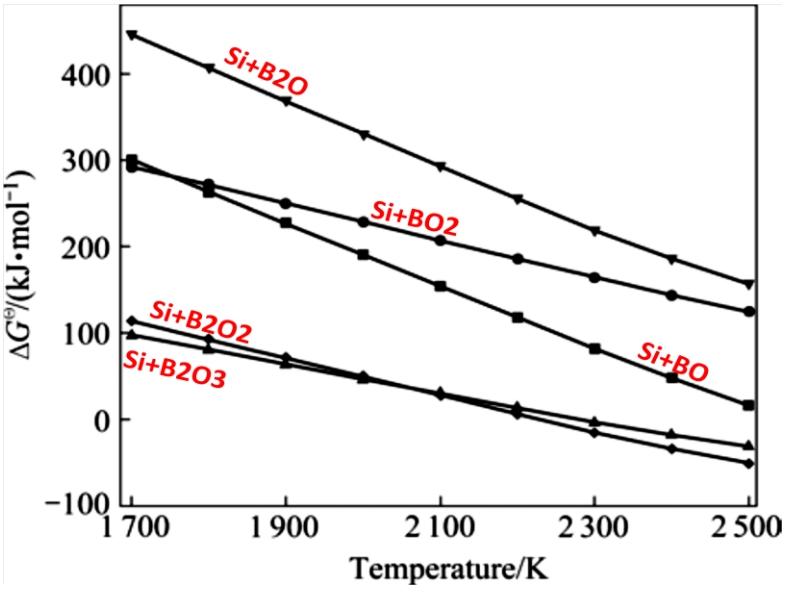


Figure 3: $\Delta G^{\ominus}$ vs temperature for reactions between $SiO_2$ and [B] per mole $SiO_2$ [33] (The pertaining products are shown on each curve.)

According to figure 4, under 2300 K, the $\Delta G^{\ominus}$ values of all reactions are positive. If we change the pressure of the system, it's possible to obtain the negative values for Gibbs free energy change. $SiO_2$ is reduced and the B is then oxidized into BxOy. The general reaction and its isothermal equation are shown in Eq. 3 and Eq. 4:

$$(SiO_2)+\frac{2x}{y}[B]=Si(l)+\frac{2}{y}(B_xO_y)(g) \qquad \text{Eq. 3}$$

$$\Delta G=\Delta G^{\ominus}+2.303RT\lg\frac{[p(B_xO_y)/p^0]^{2/y}\cdot a(Si)}{a([B])^{2x/y}\cdot a(SiO_2)} \qquad \text{Eq. 4}$$

Considering the activity of Si and $SiO_2$ equal to unity, and by assuming the activity of boron equal to $(w([B])/w^0).f([B])$, when $(w([B])/w^0)\rightarrow 0$ then the Henrian activity coefficient of boron, f([B]), equals to unity. Assuming that the reaction is equilibrated at which $w([B])/w^0 = 2\times10^{-4}$, the equilibrium partial pressure of boron oxide species vs temperature can be depicted as Figure 4:

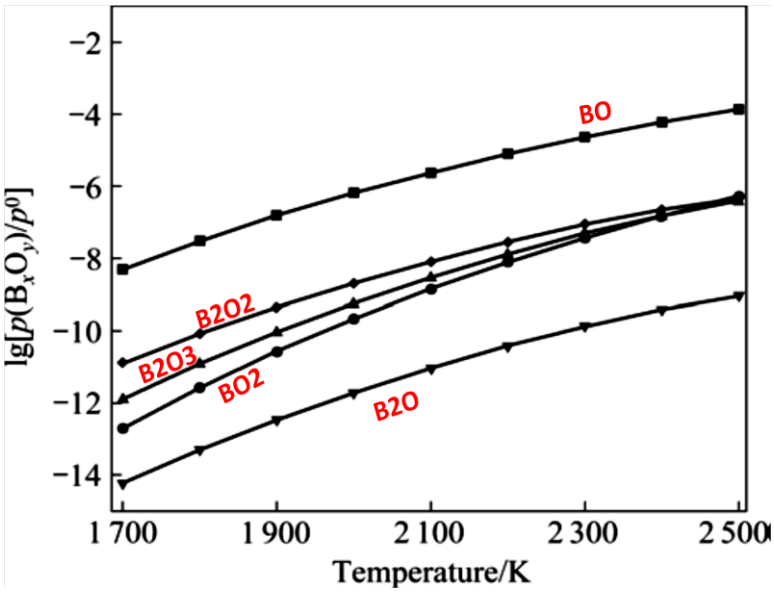


Figure 4: Equilibrium partial pressure of boron oxide species vs temperature [33]

According to the graph, in the range of 1685-2500 K, BO is the most volatile compound and its equilibrium partial pressure is about $10^{-3}$-10 Pa. The equilibrium partial pressure of boron oxide species determined in the order BO, $B_2O_2$, $B_2O_3$, $B_2O$ and $BO_2$. Therefore, by using oxygen atmosphere in the above mentioned temperature range, the B in

metallurgical grade silicon can be removed. Along with the boron removal, silicon can be recovered by reduction of SiO and $SiO_2$.

### 2.5.3. Refining by Oxygen Water Vapor

Based on the NIST-JANAF Thermochemical Tables, by using $O_2$-$H_2O$ atmosphere, the gaseous boron hydrates BHO, $BHO_2$, $BH_2O_2$, $BH_3O_3$, $B_2H_4O_4$, $B_3H_3O_3$, $B_3H_3O_6$ can be formed.

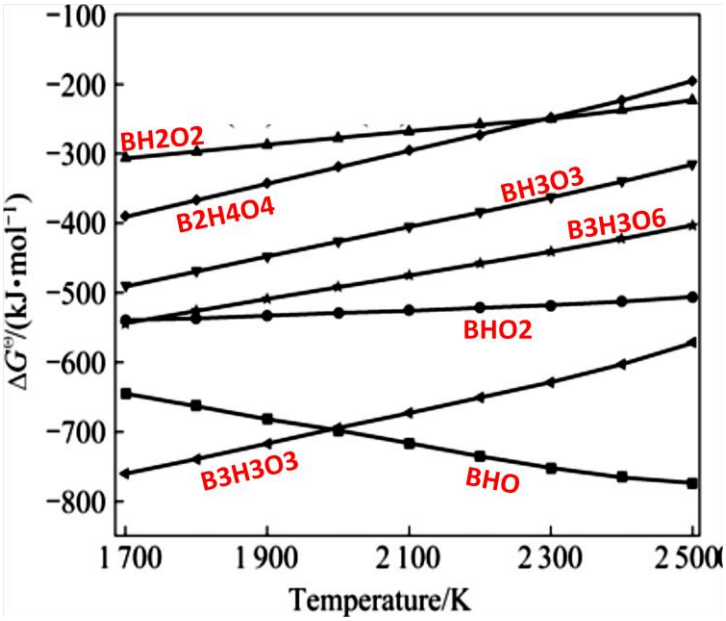


Figure 5: $\Delta G^{\ominus}$-T curves of the reactions among B, H2O and O2 [33]

According to figure 5 at temperatures below 2000 K, the most volatile boron hydrate compounds fall in the order $B_3H_3O_3$, BHO, $BHO_2$, $B_3H_3O_6$, $BH_3O_3$, $B_2H_4O_4$ and $BH_2O_2$. Also

at temperatures above 2000 K, BHO is most easily formed. The general reaction and its isothermal equation are shown in Eq. 5 and Eq. 6;

$$\frac{4x}{2y-z}[\mathrm{B}]+\frac{2z}{2y-z}\mathrm{H_2O(g)}+\mathrm{O_2}=\frac{4}{2y-z}(\mathrm{B_xH_zO_y})(\mathrm{g}) \qquad \text{Eq. 5}$$

$$\Delta G=\Delta G^{\ominus}+2.303RT\cdot\lg\frac{p(\mathrm{B_xH_zO_y})/p^0}{[p(\mathrm{H_2O})/p^0]^{2z/(2y-z)}\cdot[p(\mathrm{O_2})/p^0]\cdot a([\mathrm{B}])^{4x/(2y-z)}} \qquad \text{Eq. 6}$$

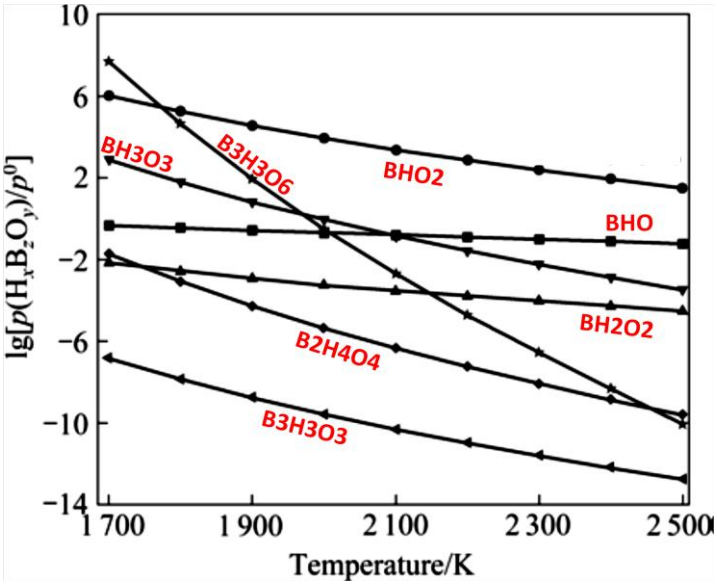


Figure 6: Partial pressure of BxHzOy versus temperature [33]

With the similar assumptions for the activities of Si, $SiO_2$ and B as in previous section, partial pressure of boron hydrates versus temperature is depicted in figure 6. In contrast to the case for boron gaseous oxides, the partial pressure of gaseous boron hydrates is decreased at higher temperature. (Behavior of BHO is an exception here.) So, for effective removal of the boron, the treatment temperature should be as low as possible but high enough to have proper viscosity for silicon melt.

Based on the thermodynamic equilibrium analysis, the rate of B removal in MG silicon with an oxygen-water vapor mixture is considerably higher than that of oxygen. Also the partial pressure of gaseous boron hydrates is much higher than that of gaseous boron oxides by 5-10 orders of magnitude. Therefore, for the oxygen treatment of MG-Si, it's better to use the oxygen water vapor mixture at lower temperature.

Wu et al. experimentally showed that in the electric arc furnace (Figure 7) with systematic total pressure of $10^{-3}$ Pa, and by oxygen-water vapor gas mixture, in the first 10 minutes, the B was decreased from 18 ppm to 2 ppm but after this period, the treatment was not effective. [33]

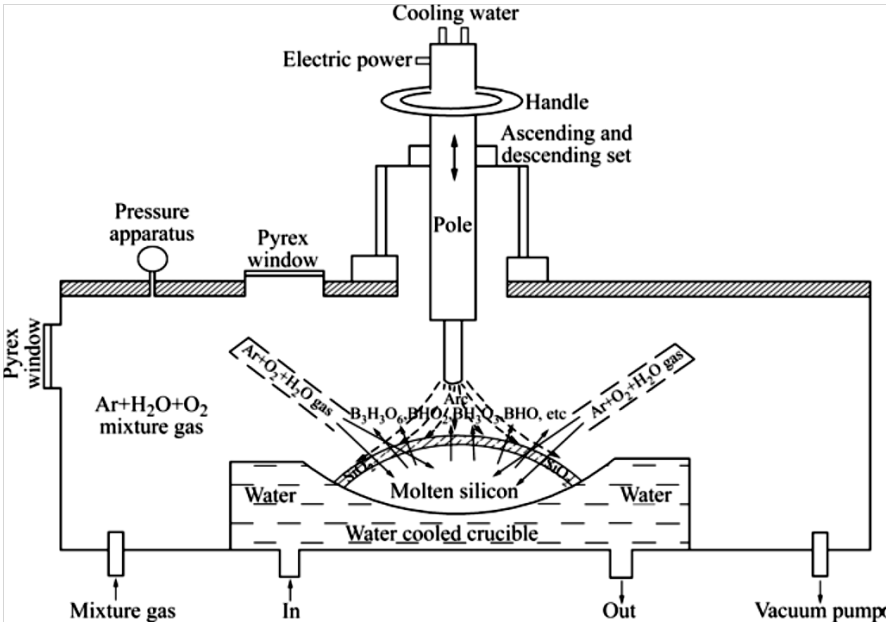


Figure 7: Electric arc furnace for boron removal [33]

## 2.6. Oxidation of impurities

Silicon can simply form chemical compounds with other elements, especially with $O_2$. Schematic diagram of $\Delta G_f$-T for oxides is shown in figure 8.

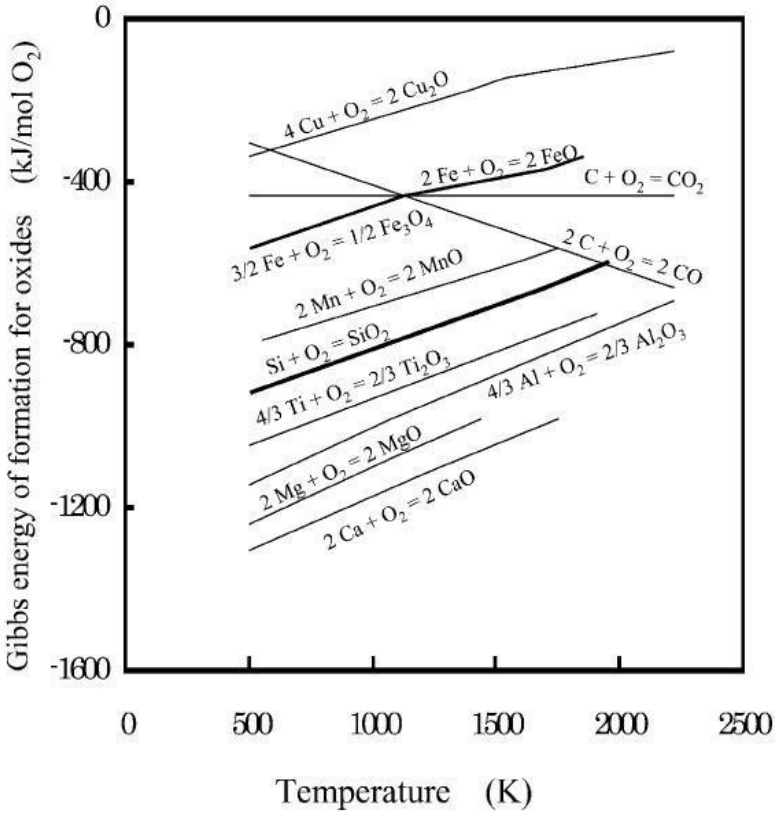


Figure 8: Gibbs energy change of oxide formation with temperature (Ellingham diagram)

The line for silicon oxidation on the Ellingham diagram lies in the middle, which shows the stability of the $SiO_2$. Therefore, reducing $SiO_2$ to produce silicon (MG-Si) is a problem compared with elements that lie in the upper part of the diagram and eventually there are restricted choices for $SiO_2$ reduction. In spite of this, impurity elements in MG silicon can be oxidized to form other compounds and removed from MG silicon in the form of a

slag. Based on calculations, it is thermodynamically possible, and then experimental conditions have to be set to allow the formation of these species. [19]

## 2.7. Slagging

Slag treatment is based on mixing Si with a chemical that has high affinity for the impurities, forms a stable compound, and can later be partitioned from the silicon through deposition on the crucible walls or filtering. A synthetic slag can be added to the charge for refining or formed as a result of reactions with impurity elements. It is important that the components of the slag not contribute impurities to silicon which cannot be removed by later processing. MG-Si contains alkali and alkaline earth elements that are slag formers. An analysis should be done to review the impurity elements and evaluate their tendency to go into the slag phase. This tendency depends on the acidity/basicity of the slag as well as the oxygen partial pressure [5].

Liquid slags are ionic in structure. Therefore the molten oxides which form the slag appear as cations and anions. These oxides appear as two major categories;

(a) Basic oxides such as CaO, FeO, MgO, $Na_2O$ and $K_2O$ that ionize (e.g. $CaO = Ca^{2+} + O^{2-}$) and donate $O^{2-}$ ions to the slag

(b) Acidic oxides such as $SiO_2$, $P_2O_5$ and $Al_2O_3$ that receive $O^{2-}$ and form bigger anions (e.g. $SiO_2 + 2O^{2-} = SiO_4^{4-}$)

Therefore, one molecule of $SiO_2$ is neutralized by two molecules of basic oxide. When the slag is consisting of these ratios of basic and acidic oxides, it is referred to be neutral

slag, i.e. $SiO_2$+CaO= $Ca_2SiO_4$ or 2CaO.$SiO_2$. A basic slag consists of more basic oxide than the neutral composition and the slag will have an excess of $O^{2-}$. Contrarily, an acidic slag consists of more acidic oxide than the neutral composition and will have an excess of e.g. $SiO_2$. [34]

Different methods are proposed to measure the basicity of slags, the most accurate one being given by the basicity ratio, where:

$$\text{Basicity ratio} = \frac{\text{Number of moles of basic oxides} - 3 \times \text{Number of moles of (Al2O3+P2O5)}}{2 \times \text{Number of moles of SiO2}} \quad \text{Eq. 6}$$

According to Eq. 6, when the ratio equals unity, the slag composition will be neutral, for less than unity, an acidic slag and greater than unity the slag composition will be basic. For simplicity, in most cases the ratio CaO/$SiO_2$ is referred as basicity ratio. [34]

Optical basicity is a measure of the average electron donor power of the oxygen ion present in the slag. As it's a measure of electron donor power, there is no need to differentiate between the slag components in terms of their acidic or basic behavior. Optical basicity was originally measured spectroscopically. It's based on the fact that electron donation to a probe ion with an electron configuration $d^{10}s^2$ results in an expansion of the outer electron layer. This expansion is proportional to the frequency of the absorption band and measured in the UV range. [40]

In refining MG silicon, boron removal is problematic. Plasma refining (coupled with water vapor and hydrogen) can be used for boron removal. However the equipment and

operation of the plasma method is expensive. Slag treatment of silicon can be another approach if a high partition ratio of the B is attainable. $CaO\text{-}SiO_2$ slag systems such as $CaO\text{-}SiO_2\text{-}CaF_2$, $CaO\text{-}SiO_2\text{-}Al_2O_3$ and $CaO\text{-}SiO_2\text{-}Al_2O_3\text{-}MgO$ are examples of candidates for B removal from Si. The amount of boron separated from the silicon melt by the slag system is a function of (a) $CaO/SiO_2$ ratio, (b) the oxygen partial pressure and (c) the state of the boron in the slag, which is related to the structure of the slag. The structure of the slag systems have not yet been investigated in detail, specially for the $CaO\text{-}SiO_2\text{-}B_2O_3$ system, but due to different applications of borosilicates with the general structure $M_2O\text{-}SiO_2\text{-}B_2O_3$, they have gained more attention.

Morita et al. [35] recently investigated $CaO\text{-}SiO_2\text{-}CaF_2$ slag systems containing 25% and 40% $CaF_2$, with different $CaO/SiO_2$ ratios from 0.3- 4 and 0.3-7 respectively. Silicon was doped with 150 ppm boron in a graphite crucible using an induction furnace. Three grams of doped Si were then equilibrated with 6.7 g of silicate slag at 1823 K. After 18 h the sample was quenched in water and chemically analyzed by ICP-AES.

The boron content in the slag and silicon and boron partition ratio in the slag was measured (Table 4).

Table 4: Initial and final composition of CaO-SiO2-25%CaF2 and CaO-SiO2-40%CaF2 slags equilibrated with silicon for 18 h at 1823 K [35]

| Initial $CaO/SiO_2$ | Final $CaO/SiO_2$ | [B] (mass ppm) | [Ca] (%) | (B) (mass ppm) | Partition |
|---|---|---|---|---|---|
| $CaO\text{-}SiO_2\text{-}25\%CaF_2$ | | | | | |
| 2.75 | 2.76 | 24.5 | 0.19 | 59.6 | 2.4 |
| 2.00 | 2.09 | 16.6 | 0.15 | 39.7 | 2.4 |
| 1.50 | 2.57 | 26.4 | 0.18 | 61.0 | 2.3 |
| 1.14 | 2.18 | 16.4 | 0.29 | 32.4 | 2.0 |
| 0.9 | 1.28 | 30.5 | 0.96 | 54.5 | 1.8 |
| 0.67 | 1.04 | 51.6 | 0.79 | 62.6 | 1.2 |
| 0.36 | 0.89 | 52.0 | 0.52 | 54.3 | 1.0 |
| $CaO\text{-}SiO_2\text{-}40\%CaF_2$ | | | | | |
| 5.00 | 2.64 | 22.6 | 2.63 | 45.7 | 2.0 |
| 3.00 | 2.26 | 31.3 | 1.73 | 45.9 | 1.5 |
| 2.00 | 1.64 | 20.1 | 2.95 | 28.3 | 1.4 |
| 1.40 | 2.12 | 36.0 | 1.22 | 57.1 | 1.6 |
| 1.00 | 2.35 | 27.9 | 0.84 | 52.2 | 1.9 |

Figure 9 shows that the addition of $CaF_2$ did not improve the partition ratio of boron. However a broader basicity range was gained compared to the binary $CaO\text{-}SiO_2$ system. Another aim behind $CaF_2$ addition is to decrease the viscosity of the slag and increase the solubility of lime.

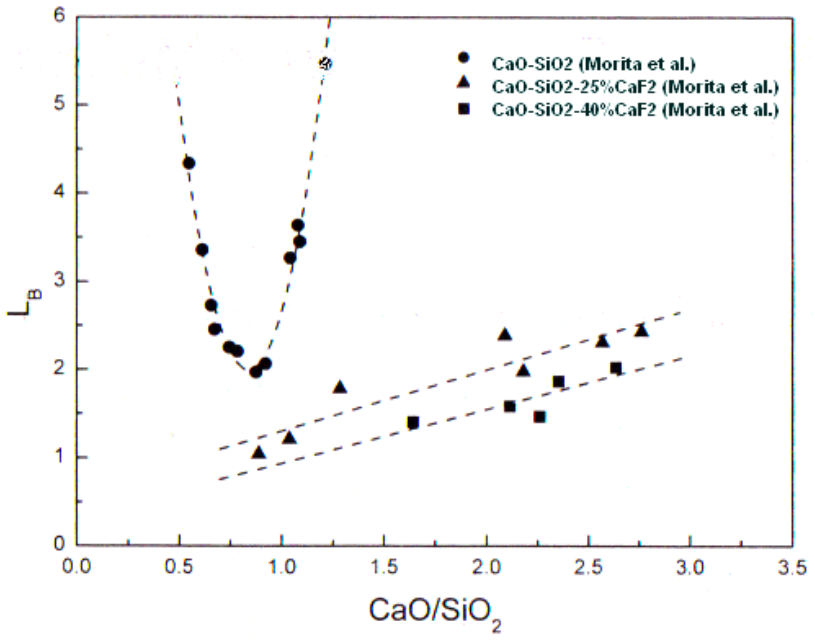


Figure 9: The boron partition ratio (LB) between the slag and the silicon phase for silicate slags as a function of the final basicity of the slag equilibrated at 1823 K [35-36]

Considering the following reaction (Eq. 7);

$$B(l) + \tfrac{3}{4}\, SiO_2 = {}^{1}/_{2}\, B_2O_3(l) + \tfrac{3}{4}\, Si(l) \qquad \text{Eq. 7}$$

The activity coefficient of boron can be calculated as Eq. 8 [37-39];

$$\log \gamma^{0}_{B(l)} = -\frac{1.1\times10^{4}}{T} + 5.82 \qquad \text{Eq. 8}$$

Figure 10 shows the relation between activity coefficient of $B_2O_3$ and basicity. The increase at $CaO/SiO_2 < 0.8$ indicates the incorporation of boron into the silicate network but at $CaO/SiO_2 > 0.8$, this coefficient decreases, indicating an increase in borate formation in the slag. The further decrease in the activity coefficient of boron oxide by adding more silica is not necessarily a function of the boron content incorporated in the

network but may be attributed to the degree of polymerization of the slag structure. [35-36]

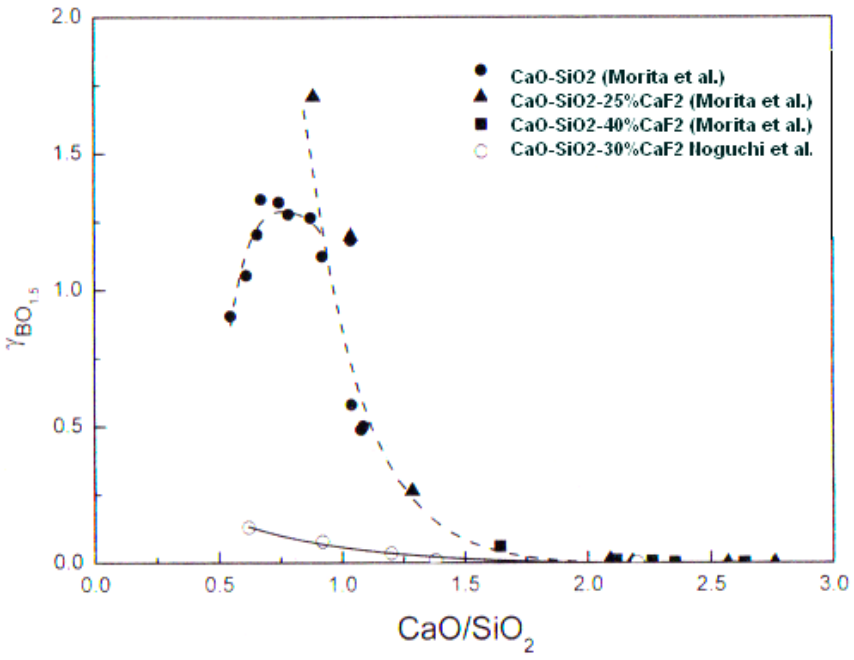


Figure 10: Relation between activity coefficient of B2O3 and basicity [35]

A detailed study on the boron coordination in $M_2O$-$SiO_2$-$B_2O_3$ glass systems was done by other scholars using 3QMAS (triple-quantum magic angle spinning) NMR and the tendency of mixing among BO4, non-ring $BO_3$, and ring $BO_3$ were investigated. The results revealed that $BO_4$ and non-ring $BO_3$ tend to mix with the silicate units, while ring $BO_3$ tends to connect to borate units. Tetrahedral boron structure ($BO_4$) has an extra bond, thus receiving a negative charge. In $Na_2O$-$SiO_2$-$B_2O_3$ glasses, this charge is

compensated by the presence of a sodium ion close to this boron. A schematic illustration of different bonds in silicate structure of the slag system is shown in fig. 11.

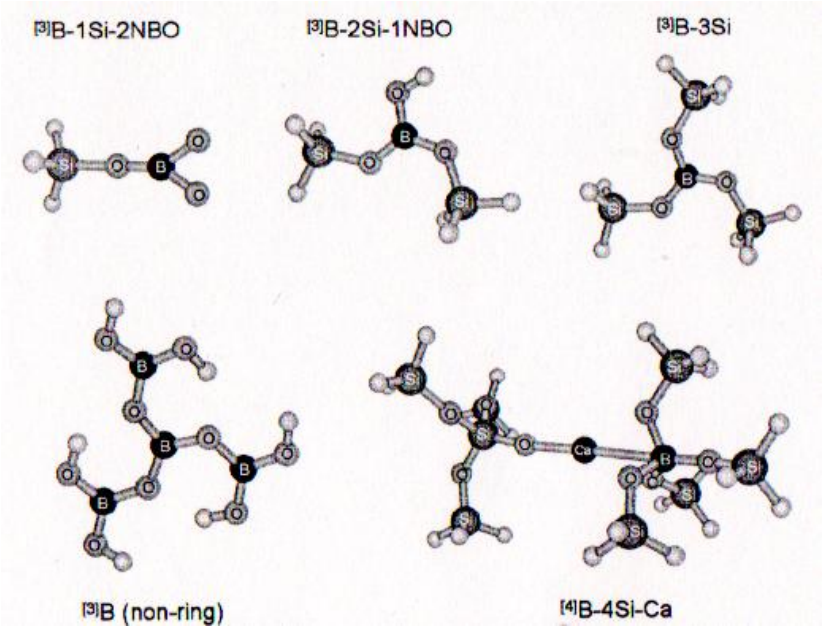


Figure 11: Schematic illustration of different bonds in silicate structure of the slag system. Here non-ring $BO_3$ and tetrahedral boron oxide are denoted as $^{[3]}B$ and $^{[4]}B$. [36]

The oxidation of boron by slag treatment can be represented by Eq. 9;

$$B + {}^{3}/_{4}\, O_2 + {}^{3}/_{2}\, O^{2-} = BO_3^{3-} \qquad \text{Eq. 9}$$

The deboronizing power of a slag can be normalized for oxide systems by borate capacity. Morita et al. assumed that the activity coefficient of the boron ion is fixed as boron is added to the slag and the activity of the oxygen ion in the slag does not depend on the oxygen potential. By providing these assumptions, borate capacity is a useful parameter to rank the deboronizing ability of the slags and is independent of experimental conditions. Based on the above equation, the borate capacity is defined by the following statement (Eq. 10) [35].

$$C_{BO_3^{3-}} = \frac{(mass\%\ BO_3^{3-})}{a_B\ P_{O_2}^{3/4}} = \frac{K\ a_{O^{2-}}^{3/2}}{f_{BO_3^{3-}}} \qquad \text{Eq. 10}$$

Logarithmic relation of borate capacity with basicity at 1823 K is depicted in figure 12.

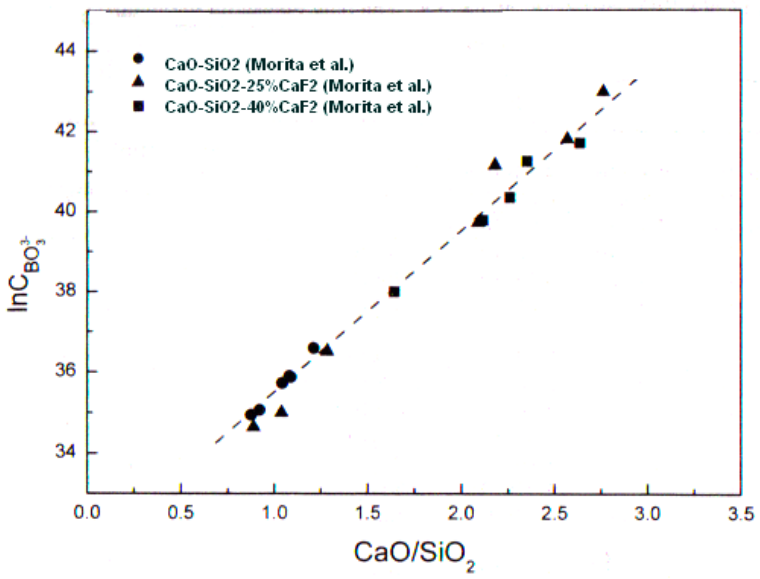


Figure 12: Logarithmic relation of borate capacity and basicity of the silicate slag at 1823 K [35]

## 2.8. Gas blowing

During the purification process of liquid MG-Si, the melt is subjected to different gases such as Ar, $N_2$, $Cl_2$, $SiCl_4$, $O_2$, $H_2$-$H_2O$, $CO_2$, or their mix. These gases can be used to react with the impurities, or to promote stirring of the liquid. They have also been used to carry solids (slags), liquids (moisture) or gases (gas mixtures) to react with liquid MG silicon and develop purification. [31,41]

## 2.9. Boron Removal by Titanium Addition

Yoshikawa and Morita investigated purification of silicon by using a Si-Al liquid and solidification method at low temperature [42-48]. Their work consisted of the following steps: making the Si-Al liquid by alloying MG silicon with Al, solidification of Si from the liquid, and acid leaching to collect purified silicon. The result showed that over 90% of boron is removed from silicon by the process. If Ti is added before the solidification of Si from the liquid, the B and Ti form a compound with high thermodynamic stability that can be removed from the Si-Al melt in the form of $TiB_2$. (Eq. 11)

$$Ti\ (l) + 2B\ (l) \rightarrow TiB_2\ (s) \qquad \text{Eq. 11}$$

For equilibrium between the eutectic liquid and TiB2, excess titanium was added to the Si-Al liquid containing B, and $TiB_2$ was precipitated. The composition of Si-Al-B alloy was Si-60 at% Al at 1273 K, Si-64.6 at% Al at 1173 K, B content: 200 to 400 ppma. About 5

grams of the alloy was equilibrated with titanium chips (99.5 %) under Ar- 10% $H_2$ gas for about 6 h in an alumina tube. Then the 5 mm thick sample was cooled and the bottom face containing $TiB_2$ precipitates was polished both mechanically and chemically. ICP-ES was used to determine the levels of boron and titanium after acid leaching (Table 5). [42]

Table 5: Impurity contents of refined Si after solidification on the Si-Al Melt with the Addition of Ti (ppma) [42]

| | Initial Contents of Si-Al Melt | | Contents of Refined Si | | |
|---|---|---|---|---|---|
| Sample | B | Ti | B | Ti | Al |
| C-01 | 106 | 82 | 5.5 | 0.61 | 605 |
| C-02 | 177 | 165 | 4.1 | 0.63 | 642 |
| C-03 | 226 | 278 | 3.7 | 0.34 | 576 |
| C-04 | 180 | 458 | 2.5 | 0.75 | 599 |
| C-05 | 212 | 571 | 1.8 | 0.40 | 497 |
| C-06 | 173 | 884 | 3.4 | 1.4 | 629 |
| C-07 | 170 | 933 | 1.1 | 1.6 | 726 |

The relationship between the Ti and B contents of the Si-Al liquid is shown in figure 13, and the temperature dependence of the solubility shows that the B can be effectively removed from the Si-Al liquid at a lower temperature.

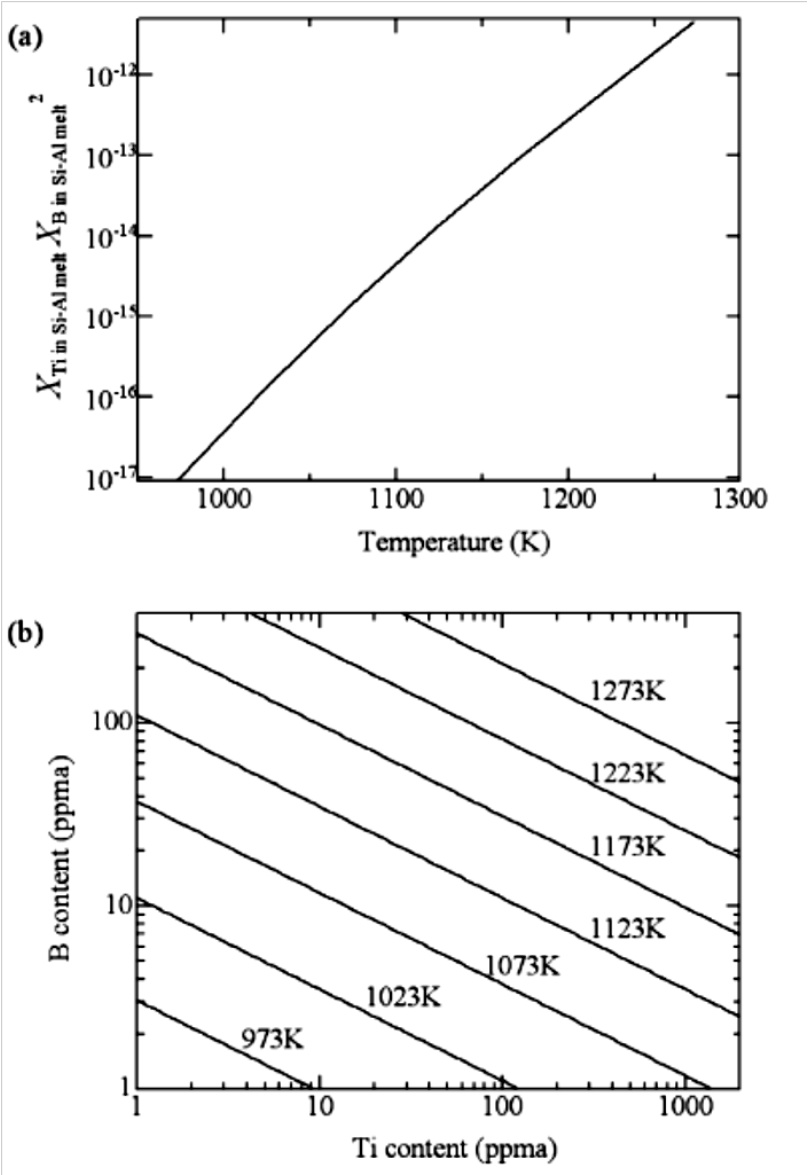


Figure 13: $TiB_2$ solubilities in the Si-Al liquid at liquidus compositions.

(a) Temperature dependence of the solubility products.

(b) Relationship between the Ti and B contents of the Si-Al liquids [42]

Since at a lower temperature $TiB_2$ has smaller solubilities in the Si-Al liquid, boron can be reduced effectively in the solidified silicon. Adding a proper amount of titanium will also improve this process. [42]

## 2.10. Simultaneous reactions

According to the theory of the above mentioned purification methods, different experimental conditions might be needed for refining different impurities. Experimentally combining the purification methods has proved even better results rather than the sum of the single processes. Here two examples of simultaneous reactions in silicon purification specially for boron refining will be reviewed.

### 2.10.1 Oxidation removal of boron by flux injection technique

Boron removal is the most difficult step in MG silicon purification due to its low vapor pressure and high segregation coefficient [49]. Plasma melting is the most promising metallurgical process that can lower the boron level from around 10 mass ppm in MG silicon to 0.1- 0.3 mass ppm in SoG silicon [50-52]. However according to the references, it takes longer than 5 hours to produce 300 kg of SoG silicon. Therefore, researchers have been investigating oxidation removal of boron from liquid silicon by several methods of flux treatment as an alternative for boron removal in plasma refining. [53-54] Based on these investigations, the boron level can be reduced to about 1 mass ppm

by injection of $CaO\text{-}CaF_2$ flux powder into the silicon melt while comparing to plasma melting, the removal rate is much faster. This “flux injection method” is a non-equilibrium purification process with injection of oxygen and highly basic flux. In this method, high oxygen partial pressure is established locally at the flux-$O_2$-Si interface. The process shown in figure 14 is proposed by Tanahashi [54] as a further low cost manufacturing process for SoG silicon. The proposed flux injection process is expected to take the role of a pretreatment step for boron removal. In this step most of the boron can be removed from silicon and energy cost of the plasma melting will be low. Another aim for flux injection is to supply Ca to the liquid Si. In order to remove Fe and Ti by acid leaching, Ca has to be pre-added to molten silicon to promote their removal. When the acid leaching step is done, the residual calcium in Si can be removed by vacuum refining due to its high vapor pressure.

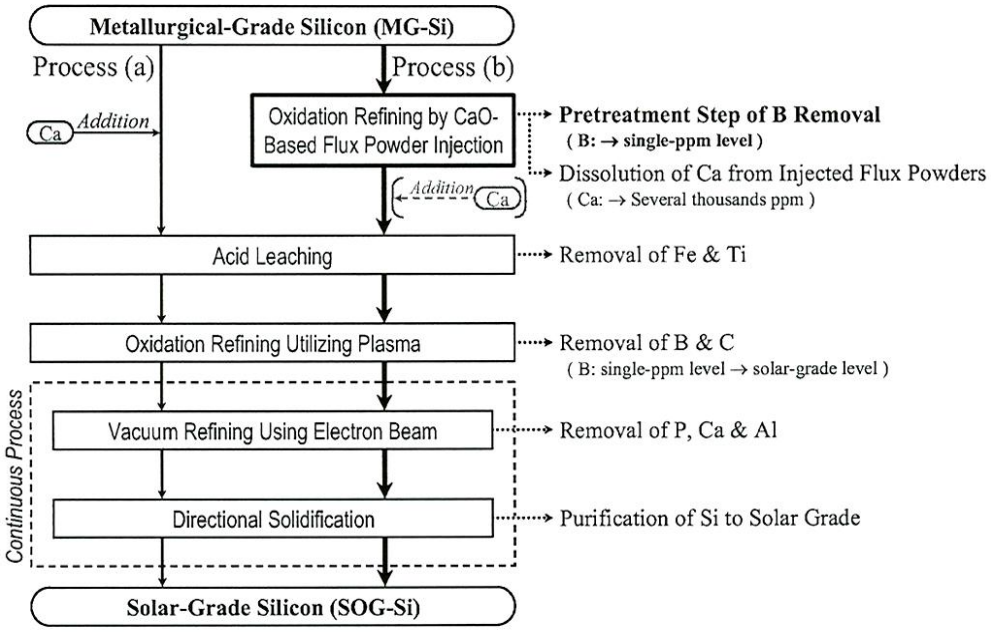


Figure 14: Flow chart of low-cost overall manufacturing process for SoG-Si from MG-Si proposed by (a) Morita, [19] (b) Tanahashi, [54]

A schematic experimental set up for the boron removal by the proposed flux injection process is shown in figure 15.

The different parameters which are controlled in this process are; operating temperature (1773 K), reaction time (30-120 sec), injection nozzle diameter (~5 mm), initial boron concentration (~8 and 15 ppm), MG silicon mass (40 g), volume flow rate of $O_2$ gas (0.9, 1.8, 3.5 and $5\times10^{-5}$ $m^3/s$), composition of injected flux powder (CaO-58 mass% $CaF_2$), injected flux powder diameter (1.5-200 µm), and flux powder mass (<23 g). [54]

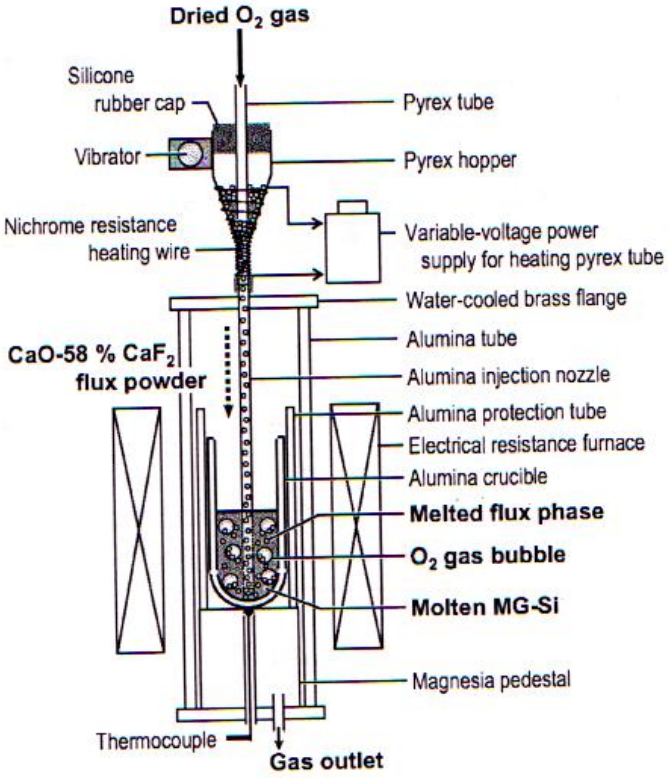


Figure 15: experimental set up for boron removal by the proposed flux injection [54]

The considerable removal of boron by oxidation occurred only in the initial stage and the rate of boron removal is controlled mainly by oxygen flow rate and injected flux rate. Boron removal rate of this process is shown in figure 16. The rate of boron removal is discussed in the reaction which occurs in the vicinity of the gas-flux exit of the injection nozzle in the molten silicon under injection conditions. The flux particle moves downward and then hits the silicon gas interface, which results in the formation of the local reaction field, flux-$O_2$-Si (figure 17). At higher oxygen flow rate and larger flux injection rate, the boron removal rate is faster. Since the basicity of the flux and oxygen

partial pressure at the flux-$O_2$-Si interface are high, the boron removal from the silicon melt to the injected flux phase is expressed by following reaction (Eq. 12); [54]

$$B(Si) + \frac{(2m-3)}{2}\ O^{2-}(flux) + \frac{3}{4}O_2(g) = BO_m^{(2m-3)-}(flux) \qquad \text{Eq. 12}$$

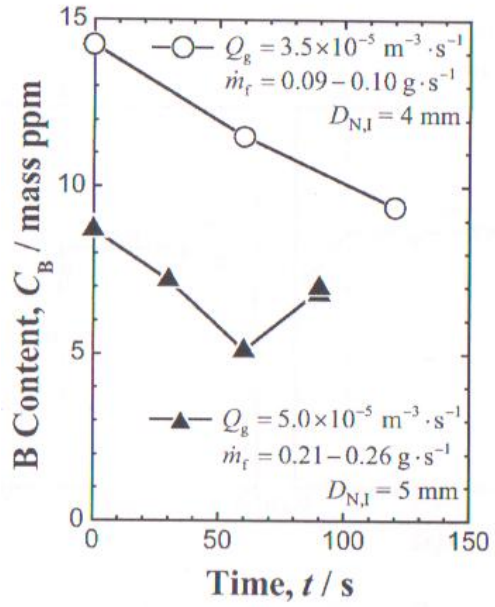


Figure 16: Time dependence of B concentration in liquid MG-Si during the flux injection process [54]

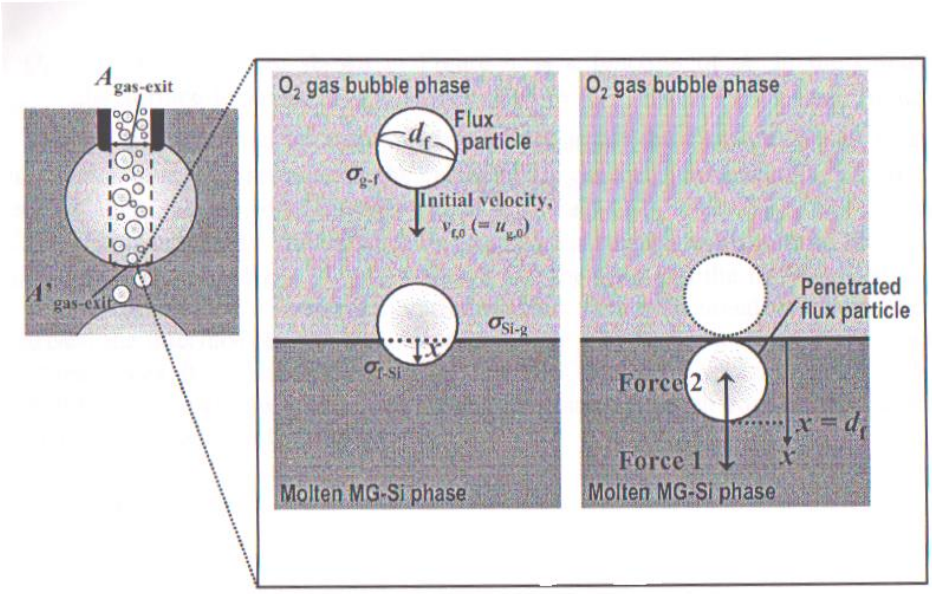


Figure 17: Schematic illustration of proposed model of local reaction field for boron removal showing penetration of the flux through the gas-Si interface [54]

According to figure 16, about half of the boron in MG-Si is removed in only 60 s under the condition of higher injection rates of oxygen and flux powder. The increase of boron concentration after 60 s is explained by the decrease of basicity of the molten flux. The boron removal in the initial stage dominates the silicon oxidation, and by increasing flux injection rate, the boron removal rate increases as well but then, not only boron but also molten MG-Si is oxidized according to the following reaction (Eq. 13);

$$Si(l) + O_2(g) = SiO_2 \text{ (in flux)} \qquad \text{Eq. 13}$$

Then the $SiO_2$ produced dissolves into the injected flux phase, which results in a notable decrease in the flux basicity due to acidic nature of $SiO_2$. At lower oxygen gas flow rates, however, the rate of boron removal was constant.

### 2.10.2 A mixed process using HEM furnace to remove boron

In another approach by Khattak et al, illustrated schematically in figure 18, the HEM (Heat Exchanger Modified) furnace was set up with combination of vacuum method and directional solidification. This approach consisted of heating the charge under vacuum to liquid state, stabilizing the liquid at 1450°C, extracting the first sample, running different purification steps with samples extracted after each step, evacuating the chamber after completion of the purification steps, and directional solidification of the charge.

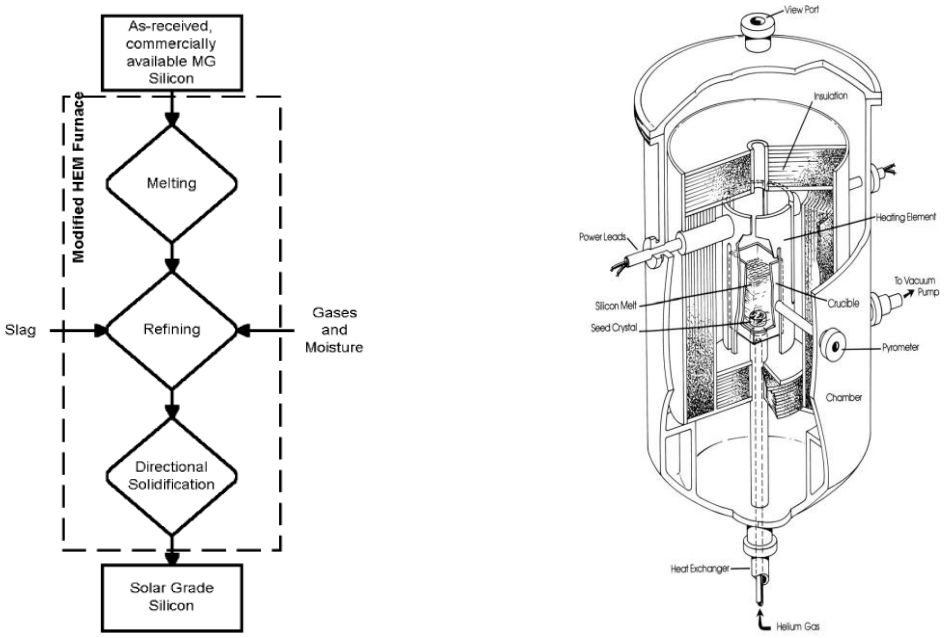


Figure 18: Using HEM furnace to upgrade MG-Si and the HEM furnace used in the process [5]

The analysis indicated that many impurity elements, besides the B were also removed during the purification step and were decreased even further after running directional solidification.

Typical impurity analysis for 140 kilogram of MG-Si charge is depicted in Figure 19. The data in this figure is normalized to the initial composition. From this data it is obvious that all impurity elements in MG silicon, including B, were decreased during the purification steps. Boron was lowered to 3.3 ppmw (~47% of the initial concentration).

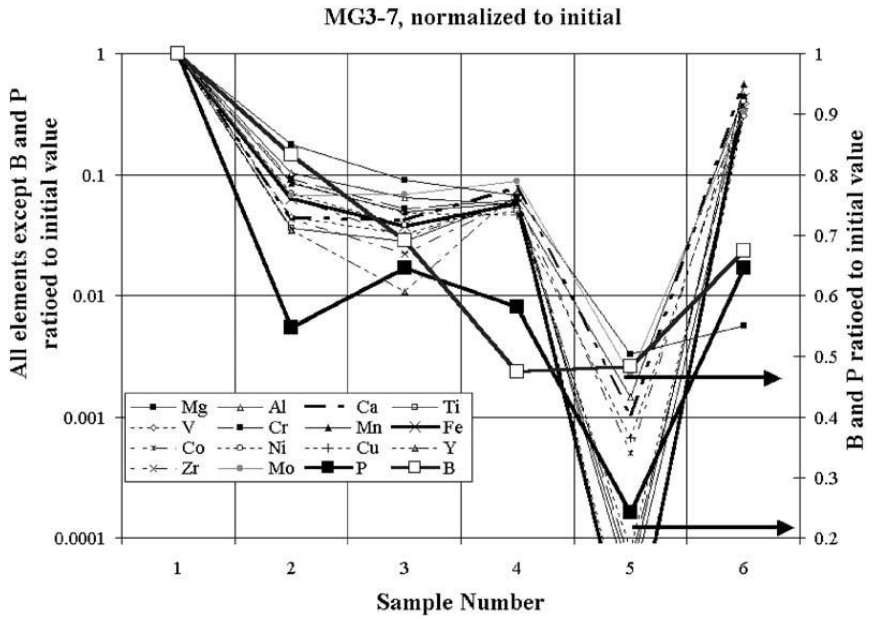


Figure 19: Analyses of samples taken during development of refining processes [5]

After making sure that boron level could be lowered in MG-Si, the next step was to improve the efficiency of the B reduction process. Similar results were reported by Khattak when they optimized the method and the charge size was increased. This is shown in figure 20, where the best B value from each experiment is reported as a function of charge size.

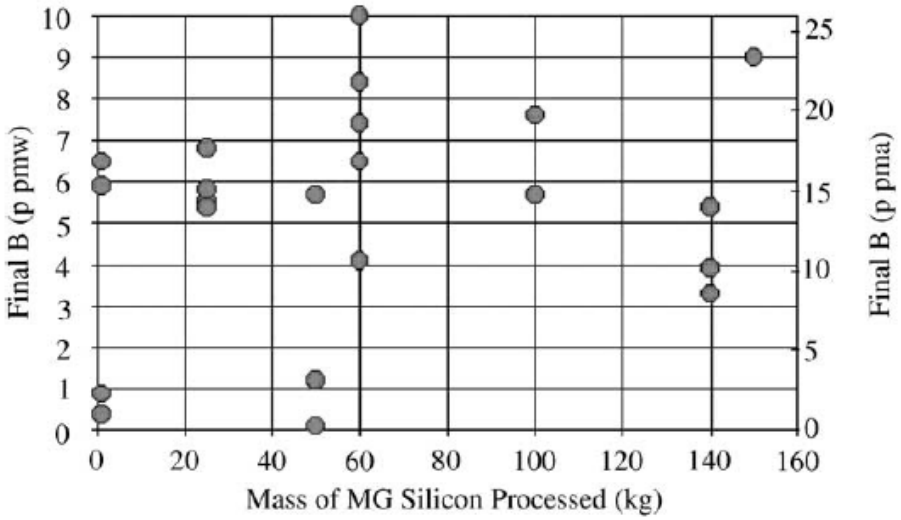


Figure 20: B concentration vs. different charge sizes after purification steps [5]

Moisturized gas blow reduced the B concentration from 20–60 ppma to below 1 ppma. After it was proved that the B can be reduced considerably, emphasis was placed on decreasing the time of purification. This experimental method led to a half-life of approximately 2 h for a 50 kg MG-Si.

## 2.11. Kinetics of impurity removal in MG silicon

In order to have a comprehensive understanding of impurity removal in MG silicon, it is necessary to consider both thermodynamics and kinetics of these processes. Thermodynamics provides information about the chemical equilibrium and the possibility of impurity removal but does not give any information on the rate of the

process. A removal process might not be favorable from the view point of kinetics. Therefore, the reaction may take much longer than what is economically viable.

Many of the removal reactions are heterogeneous i.e. they happen between several phases. For instance, the oxygen-water vapor treatment for boron removal (described in section 2.5.3) consists of reactions between gaseous phase of oxygen-water vapor and liquid MG silicon and the overall boron removal rate will depend on the transfer rate of boron to the gas-liquid interface, the reaction rate at the interface, and transfer of products away from the reaction zone. Logically, the slowest step will control the overall rate of the removal process.

### 2.11.1. Examples of the kinetics of impurity removal in MG silicon

Yuge et al. [55] investigated a new process to upgrade MG silicon. In their process, phosphorus and boron were removed in separate steps. MG silicon was melted in vacuum atmosphere to remove phosphorus. At temperatures above 1770 K and below 6.7 Pa pressure, the phosphorus content in the liquid silicon was reduced below 0.2 ppmw. The phosphorus removal reaction obeyed the first order reaction rate (Eq. 14);

$$d[P]/dt = - k'_P [P] = - k_P (A_s/V)[P] \qquad \text{Eq. 14}$$

where [P] is the phosphorus level in liquid silicon, t the time, $k'_P$ the apparent rate constant, $k_P$ the rate constant, $A_s$ the area of liquid silicon surface, and V the volume of

liquid silicon. According to that work, a decrease in atmospheric pressure, improved the removal rate of phosphorus until at very low pressures, the silicon vaporized. The phosphorus content was reduced to 0.5 ppmw in 600 min. In another attempt by Safarian and Tangstad [56], it was confirmed that the phosphorus vacuum removal in MG silicon is a first order reaction. They reported that the mass transfer of phosphorus in liquid silicon is not the rate determining step in inductively stirred liquid silicon. Based on their results, phosphorus removal under 0.5 Pa pressure is controlled by chemical reaction and mass transfer of phosphorus away from liquid surface. Also their results showed that under medium vacuum conditions and higher removal temperatures, the mass transport of phosphorus away from reaction zone is more likely to be rate determining than the chemical reaction.

In another removal step carried out by Huge et al. on MG silicon, boron was removed by applying Ar plasma plus water vapor to the liquid silicon. By using plasma treatment, the boron level reduced from about 30 ppmw to under 0.1 ppmw by formation of boron oxide and hydroxide vapor. Boron removal occurred through first rate reaction similar to Eq. 13. The removal rate of boron was a function of water vapor content in the plasma gas and reaction surface area, $A_s$ which was formed by plasma jet. The boron removal was well behaved up to 7.2% water vapor but beyond this level, the removal development ceased due to formation of a silica film on the liquid silicon surface. A graph of boron level change in the liquid silicon after plasma treatment at different

water vapor contents is shown in figure 21. The values on the graph refer to volume percentage of the water vapor used in the treatment.

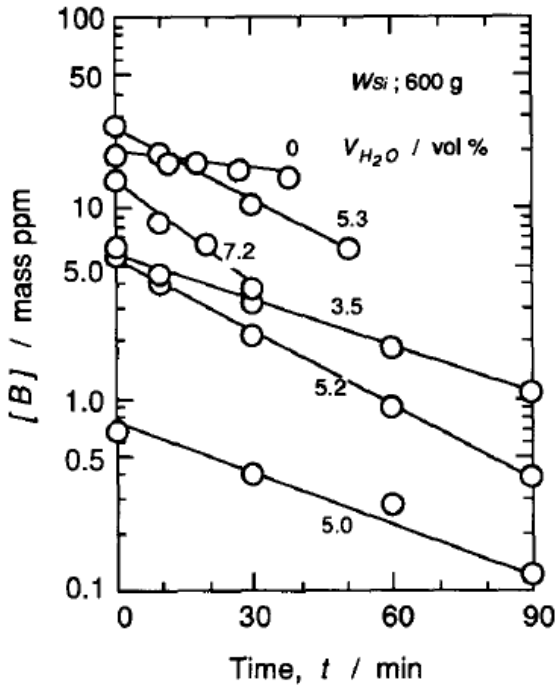


Figure 21: boron level change in the liquid silicon after the plasma treatment. The values on the graph refer to volume percentage of the used water vapor [55]

Ikeda et al. [57] also investigated development of plasma treatment of MG silicon. Their results showed that boron removal obeyed the first rate reaction similar to one in Eq. 14. They reported that the rate constant was not dependent on the $H_2O$ content up to 0.3 vol% but at increasing water vapor content up to 1.24 vol%, the removal rate increased. The influence of water vapor content on the removal rate is shown in figure 22.

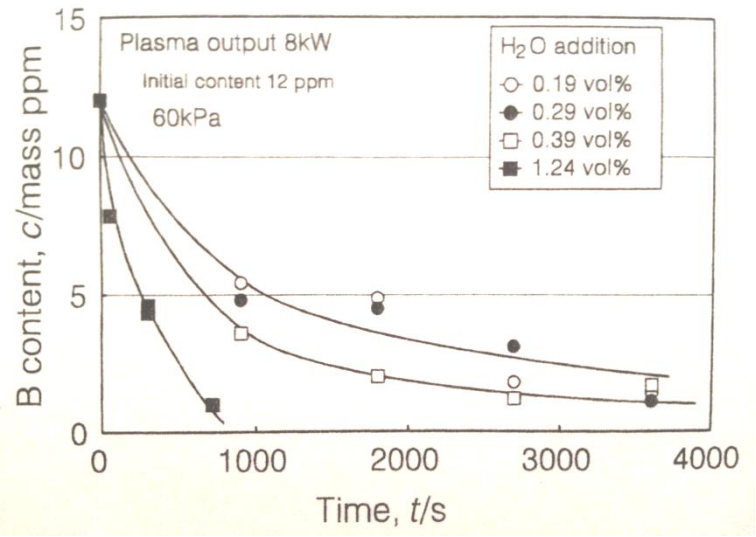


Figure 22: Influence of water vapor content on the removal rate in plasma treatment [57]

The silicon loss was also measured by Ikeda et al. They reported 6% silicon loss at $H_2O$ under 0.39 vol% that was three times the loss measured for the treatment under pure Ar. The silicon loss rate was 1.2 wt% for a melting period of 10 min which was consistent with the result reported by Suzuki et al. [58] for the similar vapor pressure of water vapor in the plasma treatment. The rate of silicon loss versus treatment time is shown in figure 23.

The silicon loss could be explained by Eq. 15 and Eq. 16 where silicon at the surface of the liquid is oxidized to liquid $SiO_2$ (Eq. 15). Then according to Eq. 16, it will react with liquid silicon to form SiO (g). The $\Delta G$ value for SiO (g) formation from Si (l) and $H_2O$ is positive that's why in Eq. 15 liquid $SiO_2$ is formed first.

$$Si\ (l) + 2\ H_2O\ (g) = SiO_2\ (l) + 2\ H_2 \qquad \text{Eq. 15}$$

$$SiO_2\ (l) + Si\ (l) = 2\ SiO\ (g) \qquad \text{Eq. 16}$$

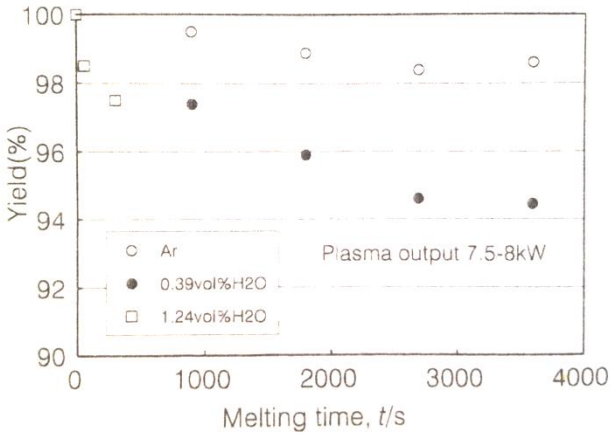


Figure 23: The rate of Si loss versus plasma treatment time [57]

More recently Tang et al. [59] investigated the kinetics of boron removal by hydrogen-water vapor. Their work followed on Theuerer's work in 1956 [32]. They reported that the boron removal rate is a first order reaction and is a function of the partial pressure of water vapor. (Eq. 17);

$$\log\frac{B}{B_0} = -kt\sqrt{P_{H_2O}} \qquad \text{Eq. 17}$$

where B is the boron concentration in the liquid silicon after the treatment, $B_0$ is the initial concentration, $P_{H_2O}$ is the partial pressure of $H_2O$, t is the time and k is the apparent rate constant.

The content of water vapor was fixed at 3.17% in the gas mixture and the process was done at 1450°C and 1500°C. The process consisted of the oxidation of both boron and silicon during the $H_2$-$H_2O$ treatment. They reported that the chamber of the furnace was covered with a white layer of $SiO_2$. According to their results, silicon recovery rates were 89% and 91% at temperatures 1450°C and 1500°C, respectively.

During the gas treatment (t= 180 min), boron level was lowered from 52 ppmw to 0.7 ppmw and 3.4 ppmw at 1500°C and 1450°C, respectively. The boron removal trend during the $H_2$-$H_2O$ gas treatment is shown in figure 24.

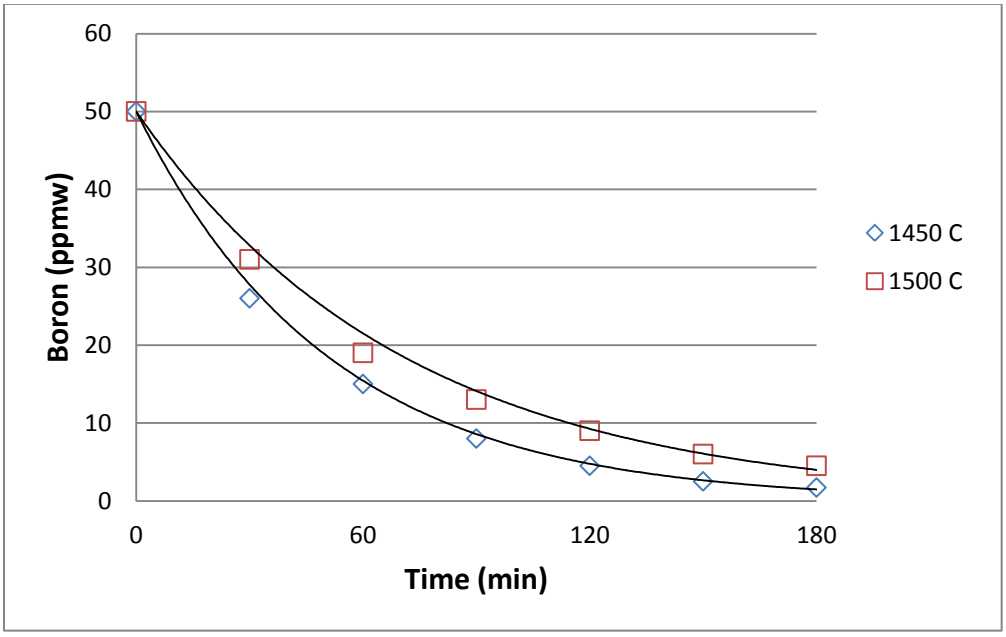


Figure 24: Boron removal trend during the $H_2$-$H_2O$ gas treatment (1450°C, 1500°C) [59]

As seen in figure 24, the rate of boron removal is faster at 1450°C. Tang et al. reported that the kinetics of boron removal by the hydrogen-water vapor gas mixture was determined by chemical reactions at the gas-liquid interface. This will be discussed later in the results and discussion chapter.

## 2.12. Summary

In recent decades many efforts have been done to obtain reliable metallurgical methods for production of SoG silicon from MG silicon. Some of the most common refining techniques currently being used, are directional solidification, vacuum treatment of the melt, chemical reaction to form volatile species of impurities, oxidation to form separate oxide phases, and slag treatment of impurities. Removal of impurities from a silicon melt first requires a reaction, such as oxidation, to form an impurity species, and then partitioning of the species from molten silicon into another phase. The most favorable technique to produce SoG silicon is by removing impurities, such as boron, aluminum and phosphorus in the molten metallurgical grade silicon, followed by directional solidification. According to the theory of the above mentioned purification methods, different experimental conditions might be needed for refining different impurities. Experimentally combining the purification methods has proved even better results rather than the sum of the single processes.

When the impurities can be reacted to form volatile molecular species, impurity elements can be eliminated through evaporation by injecting chlorine, oxygen, wet hydrogen, $SiCl_4$, $CO_2$, or their combinations. Reaction of these gases with impurity elements in liquid silicon and formation of volatile species that evaporate from the liquid, results in considerable removal. The kinetic behavior of Al removal by the chlorination treatment will be addressed in the current study.

# 3. Experiments and Materials

In this research, the chlorination treatment to remove Al from MG-Si is investigated. It was shown earlier in figure 1 that Al content can be reduced down to the required range for SoG-Si (<0.1 ppmw) by repeating conventional directional solidification twice. Since the energy cost is of great importance, it is needed to develop other cost effective methods. In this chapter, the experimental procedure of the chlorination process and the materials used are presented. The chapter is divided into two sections: removal of aluminum by chlorination and determination of Al removal rate.

## 3.1. Experimental Procedure: Al removal by chlorination process

In this process, MG silicon was melted in an alumina crucible in an argon protected tube furnace at 1450$^{o}$C. An Ar+$SiCl_4$ gas mixture was blown onto the surface or injected into the silicon melt by means of an alumina tube with 6 mm ID. (Figure 25)

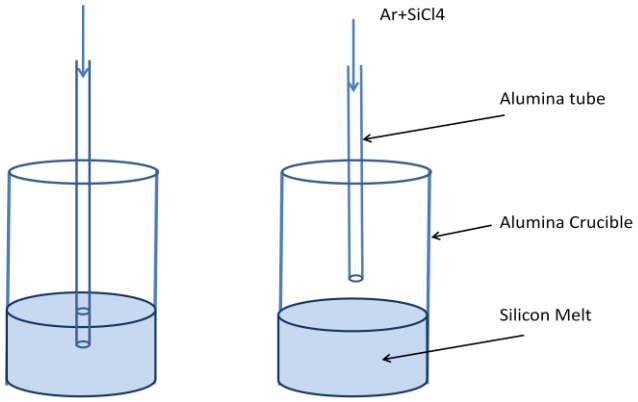


Figure 25: Schematic of two different chlorination processes on silicon melt: injection method (left) blowing method (right)

A schematic diagram of the chlorination process is illustrated in fig 26.

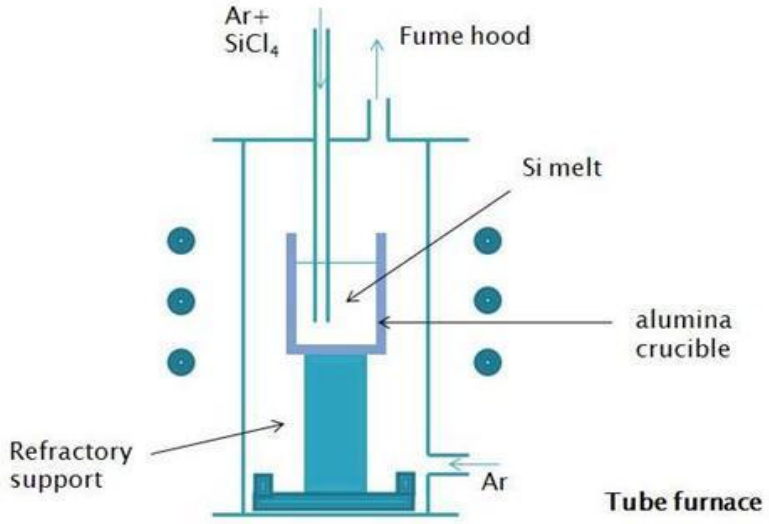


Figure 26: Chlorination process for Al removal

### 3.1.1. Materials

A graph of MG silicon chunks provided by 6N silicon is shown in figure 27. The silicon chunks were then crushed into small pieces for melting purposes.

(a) (b)

Figure 27: MG silicon used for the experiments (a) as received (b) crushed

Also chemical analysis of the major impurities in the as received MG silicon is given in table 6.

Table 6: Chemical analysis of the major impurities in as received MG silicon provided by 6N Silicon

| Impurity | Mass (ppm) |
|---|---|
| Boron | 4.5 |
| Phosphorus | 49.5 |
| Aluminum | 708.5 |
| Iron | 960.6 |
| Titanium | 106.4 |

High alumina cylindrical crucibles (99.8%) produced by McDanel Advanced Ceramics with a capacity of 50 ml (OD: 35 mm and H: 64 mm), were used for silicon melting in the experiments. (Figure 28)

Figure 28: High alumina crucible used for the experiments

### 3.1.2. Melting and Chlorination of MG silicon

A tube furnace was used in our high temperature experiments (figure 29), heated by Kanthal Super 1800 molybdenum disilicide ($MoSi_2$) elements. An alumina tube (ID: 79.4 mm, OD: 88.9 mm, Hi: 762 mm) produced by McDanel Advanced Ceramics was installed inside the furnace. The ends of the alumina tube were sealed properly using O-rings and metal caps, which were water cooled during the experiments.

To control the temperature of the furnace, a programmable EUROTHERM Power Controller was used. The furnace had a B type thermocouple (Pt- 6%Rh vs. Pt- 30%Rh). This thermocouple was connected to a digital display on the furnace control box. Since

the temperature shown by digital display and the real temperature in the hot zone of the furnace could be different, a temperature calibration was done before starting the experiments.

Figure 29: Tube furnace used for the experiments

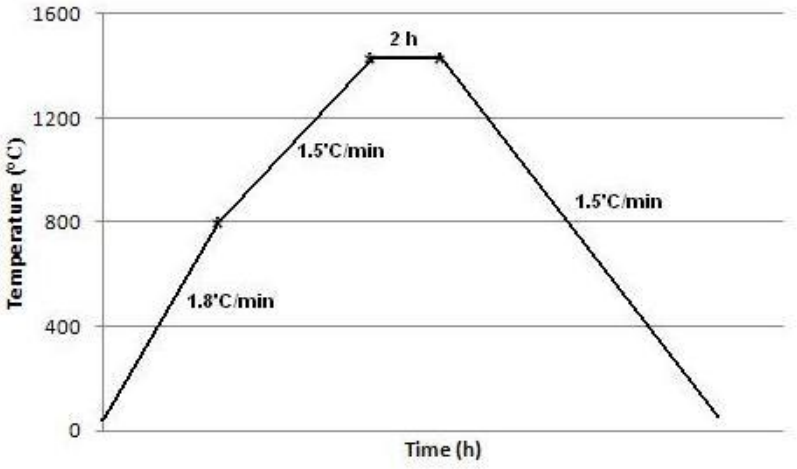


Figure 30: Schematic thermal cycle used for the experiments

The crucible containing about 35 g MG silicon was placed in the furnace and according to the thermal cycle shown in figure 30, heated at a rate of 1.8°C/min up to 800°C, and then at 1.5°C/min up to 1450°C, and held for an hour for homogenization of the silicon melt. During the process, high purity argon with a flow rate of 300 mL/min was used to flush out oxygen. In the next step, carrier argon at a flow rate of 200 mL/min was passed through liquid silicon tetrachloride and the gas mixture ($Ar+SiCl_{4)}$ was delivered to the melt either by blowing or injection as stated in figure 25 for duration of one hour. From mass balance over one hour flow, the volume percentage of $SiCl_4$ in carrier argon was %0.33. This value was calculated by measuring the volume of Ar gas and liquid $SiCl_4$ consumed during the chlorination treatment. The furnace was then cooled down and the treated MG silicon was analyzed by ICP-OES. The experimental parameters for the chlorination process are summarized in table 7.

Table 7: Experimental parameters in chlorination process

| |
|---|
| Temperature= 1450°C & Time= 1 hr |
| MG Silicon mass: ~ 35 g |
| Reactant Gas: Ar-0.33 vol% $SiCl_4$ |
| Initial Al concentration: ~700-1500 ppmw |
| Flow rate of protective Ar: 300 mL/min |
| Flow rate of carrier Ar: 200 mL/min |

The chlorine compound used for the experiments was 99% $SiCl_4$, a colorless volatile liquid with boiling point of 57.65 °C that fumes in air. A quartz tube

(OD: 40 mm, H: 300 mm) was designed as the $SiCl_4$ dispenser and sealed well with proper metal fittings. At the core of this dispenser, a porous frit was attached to one end of a smaller quartz tube (OD: 10 mm, H: 280 mm) and the other end was connected to the high purity argon source to inject fine bubbles of Ar gas into liquid $SiCl_4$. The whole container was wrapped with a transparent tape for the safety in case of breakage. During the chlorination treatments, a mixture of the Ar and $SiCl_4$ with a controllable flow rate was applied to the silicon melt. (Figure 31)

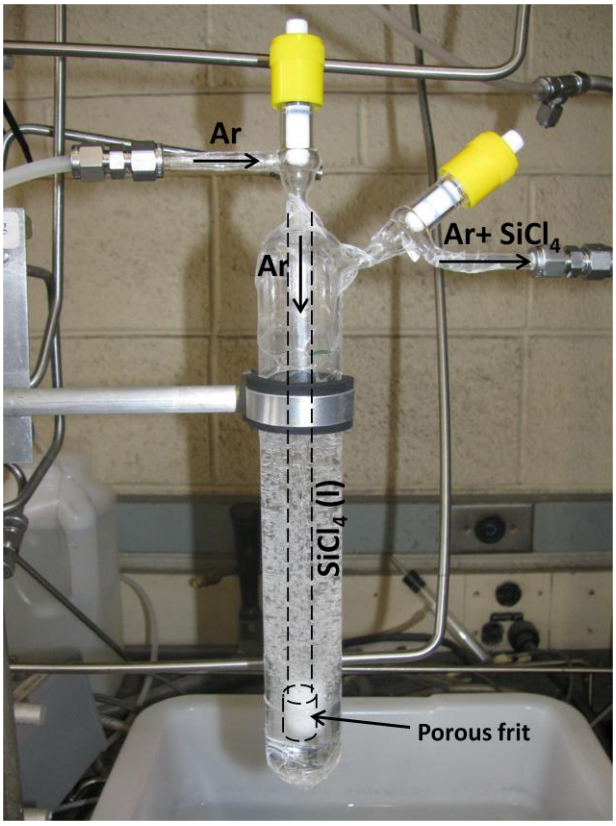


Figure 31: $SiCl_4$ container for the chlorination process

## 3.2. Experimental Procedure: Determination of Al removal rate

The conditions for the experiment were the same as previous chlorination treatment (table 7) except for the sampling stages and the chemical analysis of silicon flakes. Reactant gas (Ar plus SiCl4) was blown onto the surface of the melt for 15 minutes then stopped during sampling. The protective Ar gas was set to "open" on flow-meter controller during this time (1000 mL/min: the highest flow rate defined for flow-meter), to minimize the risk of air entering the furnace. Then chlorination treatment proceeded in intervals of 15 min. After each treatment, samples were taken by quartz tube in the amount of 1-2 ml for ICP analysis.

### 3.2.1. Materials

To investigate the removal rate of aluminum from the silicon, high purity silicon flakes were used for the rest of the experiments instead of the MG-Si used previously. These flakes have higher Al impurity because they are grown from Al-Si melt. This allowed a more accurate determination of aluminum removal rate. The chemical analysis of important impurities in the silicon flakes is given in table 8.

Table 8: Chemical analysis of the major impurities in silicon flakes provided by 6N Silicon

| Impurity | Mass (ppm) |
|---|---|
| Boron | 0.4 |
| Phosphorus | 4.3 |
| Aluminum | 3956 |
| Iron | 10.5 |

### 3.2.2. Melting and Chlorination of silicon flakes

Schematic of the furnace set up for the second part of the experiments is illustrated in figure 32. Since sampling of the liquid silicon was required during the furnace run, the top metal cap was designed differently. As shown, it contained of two parts (figure 32); the left part is for positioning an alumina tube (ID: 6mm) to direct $Ar+SiCl_4$ gas into the furnace and the right part is a branch tee (ID: 20 mm) for sampling and to release gases to the fume hood.

The sampling tube was positioned in the core of the branch tee and was properly sealed with O-ring and metal fittings. Since there was enough gap around the sampling tube inside the branch tee, the outgoing gases could easily exit the furnace. Also by using this branch tee for both sampling and as the outgoing gases path, the risk of air penetration into the furnace was minimized, because the penetrating air was flowing countercurrent to the outgoing gases.

The end part of the sampling tube was kept above the crucible before complete melting of the silicon. Then after each step of the chlorination treatment, the tube was inserted into the melt and samples were taken.

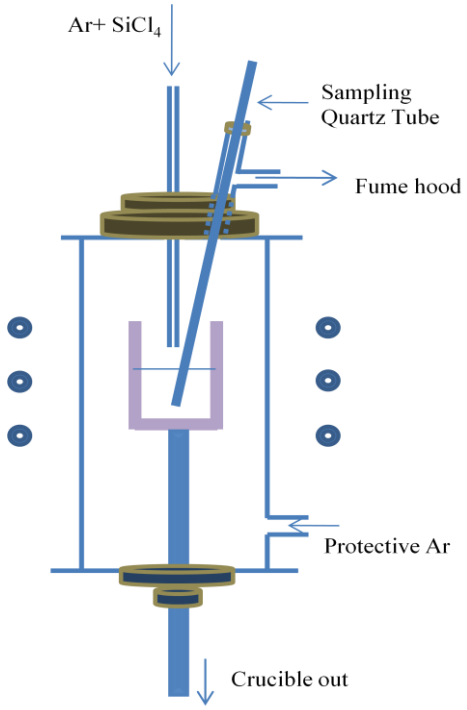


Figure 32: Schematic of the apparatus for determining Al removal rate

## 3.3. Characterization of refined silicon by ICP-OES

The Inductively Coupled Plasma - Optical Emission Spectrophotometer (ICP-OES) was used for analysis of the impurities in silicon. It features a uniquely designed CCD camera as a detector with a very wide range of available wavelengths, a grating or wavelength

selector, and powerful software to capture and analyze the data (figure 33). This instrument is configured for liquid samples only.


Figure 33: ICP-OES apparatus used in the MSE department at McMaster University

### 3.3.1. Digestion of Samples

Most metal samples can be digested with either HCl or $HNO_3$, or about a 3 HCl to 2 $HNO_3$ mixture called aqua regia. If the sample is expected to have more than about 1% Si, then a few drops of HF should be added to the acid mixture, and the digestion temperature kept low to avoid losses of $Si_2F_6$. This compound is in the gaseous state at ambient conditions. $H_3BO_3$ will complex the $Si_2F_6$ preventing this loss and avoiding precipitation of some insoluble fluoride salts such as $AlF_3$. A small excess of $H_3BO_3$ is

needed, usually about 0.2 g for a sample size of 0.1 g. A high purity $H_3BO_3$ salt is available to avoid contamination.

### 3.3.2. Silicon Digestion

The following procedure is used for the digestion of silicon:

- Weigh the samples ranging in weight from 0.1 to 0.5 g
- Add the following reagents: HF= 7 ml, $HNO_3$= 2 ml, $H_2O$= 6 ml
- Place the vessel into the microwave digester
- Run the microwave digester:
  - 15 minutes to 130°C
  - Hold for 5 minutes @ 130°C.
  - Increase to 190°C (10 minutes)
  - Hold for 100 minutes @ 190°C
- Wait for the crucible to cool to room temperature. This will ensure that the pressure is low inside the crucible. There should be no precipitate on the bottom.
- Put 10–15 ml of 5% $HNO_3$ before pouring sample into flask. This will help prevent precipitation.

### 3.3.3. Microwave Digester

Due to the nature of the samples, a microwave digester must be used for silicon digestion. The microwave digester used in our research was Milestone Ethos microwave that can safely digest solid samples at temperatures and pressures well above the normal atmospheric boiling point. This greatly reduces the digestion time, and the loss of volatile components such as silicon-flouride compounds. A picture of the microwave digester is shown in figure 34. The microwave is equipped with a rotor which can accommodate up to 10 high pressure vessels. These vessels can withstand temperatures as high as 250$^{o}$C and pressures up to 1000 psi.

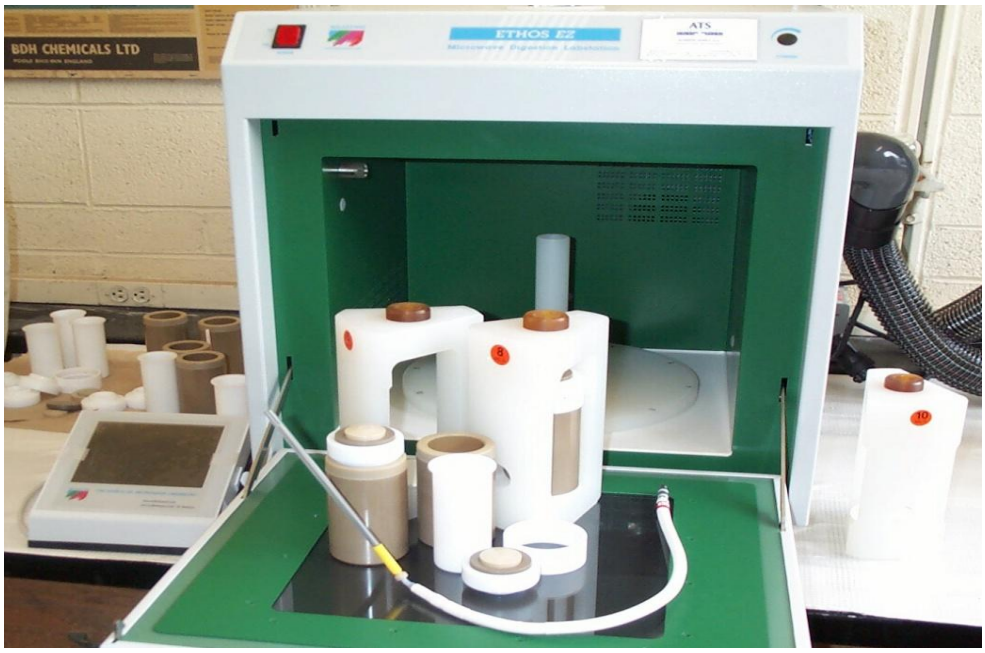


Figure 34: Milestone Ethos microwave used for digestion of silicon samples

### 3.3.4. Preparation of Standard Solutions

Four Eppendorf auto-pipettes that cover a wide range of volumes, from 0.001 to 10 mls were used for standard solutions. Three standards and one blank solution were prepared for the characterization. Table 9 lists the composition of standard solutions prepared for ICP testing.

Table 9: Standard solutions prepared for ICP test on refined silicon

| Solutions | Si | Al | B | P | $HNO_3$ | HF | $H_2O$ |
|---|---|---|---|---|---|---|---|
| Blank | - | - | - | - | 2 ml | 7 ml | 91 ml |
| Standard #1 | 50 ml | 0.01 | 0.01 | 0.01 | 2 ml | 7 ml | 40.97 ml |
| Standard #2 | 50 ml | 0.5 | 0.05 | 0.5 | 2 ml | 7 ml | 39.95 ml |
| Standard #3 | 50 ml | 1 | 0.1 | 1 | 2 ml | 7 ml | 38.9 ml |

### 3.3.5. Comparison of the ICP analysis at McMaster and 6N silicon

A comparison of ICP analysis at McMaster University and 6N silicon for a set of experiments is shown in figure 35. The chlorination parameters were the same as previous experiments stated in table 7. The comparison confirmed that the results obtained in our department were consistent with those of 6N silicon. Each point shown in the plots was the average of three points. Positive and negative error values were the maximum minus average and average minus minimum values, respectively.

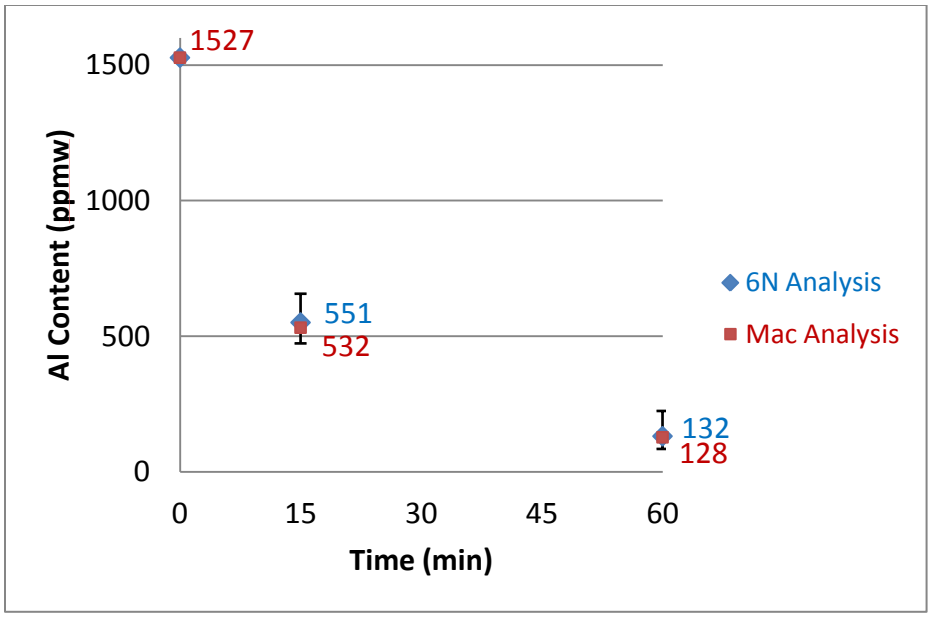


Figure 35: A comparison of the ICP analysis at McMaster University and 6N Silicon (Al removal rate in the chlorination treatment of MG silicon at 1450°C)

# 4. Results and discussion

As stated in chapter two, the chlorination process is based on the reactivity of the impurities in liquid silicon towards halogens such as chlorine or hydrogen halides to form volatile halides. In this work, the purification of metallurgical silicon by the treatment of the melt with silicon tetrachloride has been investigated. Due to the high temperature used, the local equilibrium at the melt/gas interface is presumably established at the reaction zone during the treatment.

## 4.1. Calculations by Factsage

Products of the chlorination process were determined through FactSage, a thermochemical software and databases. Assuming that the initial content of the reactants was: 1 mole silicon, 1E-3 mole aluminum, 1E-5 mole boron and 1E-3 mole $SiCl_4$, several chlorination steps was calculated at 1450°C, 1 atm. The total molar content of gaseous species and their mole fractions are summarized in table 10. Moreover, these steps were aimed at cyclical process to limit the silicon loss from the system.

Table 10: Al removal steps calculated by Factsage for chlorination process of MG silicon

Si (l) + 1E-3 Al (l) + 1E-5 B (l) + 1E-3 $SiCl_4$ (g) $\xrightarrow{1450°C,\ 1\ atm}$ products

| Step | Liquid phase | | | Molar fraction of major gaseous product species after each chlorination step | | | Total gaseous product (mole) |
|---|---|---|---|---|---|---|---|
| | $Si/Si_{Initial}$ (%) | Al (ppm) | B (ppm) | $AlCl_3$ | $SiCl_2$ | $BCl_3$ | |
| 1 | 99.887 | 238 | 7 | 0.37 | 0.46 | 1.7 E-3 | 1.52 E-3 |
| 2 | 99.827 | 32 | 2 | 0.12 | 0.59 | 3.5 E-3 | 1.60 E-3 |
| 3 | 99.765 | 4.8 | 0.7 | 2.0 E-2 | 0.65 | 5.7 E-4 | 1.62 E-3 |
| 4 | 99.706 | 0.5 | 0.25 | 2.2 E-3 | 0.66 | 4.1 E-4 | 1.63 E-3 |

These calculations confirm the feasibility of Al removal in repeated steps of chlorination. After each step, the purified silicon with certain Al content is considered as the silicon source for further refinement in the next step. As chlorination proceeds and Al concentration decreases in the liquid silicon, the fraction of $AlCl_3$ in the gas product phase decreases. Conversely, the share of silicon chloride species increases.

Table 11: Comparison of the activity coefficient of Al and B measured experimentally and calculated through factsage

| | Al | B |
|---|---|---|
| Experimental results | $\text{Ln}\,\gamma_{Al(l)} = -\frac{3610}{T} + 0.452$ [19] (T= 1723 K) $\gamma_{Al} \approx 0.2$ | $\text{Log}\,\gamma_{B(l)} = -\frac{1.11\times10^4}{T} + 5.82$ [37] (T= 1723 K) $\gamma_{B} \approx 0.5$ |
| Factsage calculations | 0.36 | 3.7 |

The activity coefficient of Al and B in liquid silicon was calculated through Factsage and compared to the experimental values obtained by other researchers [19, 37] (Table 11). Since the calculated activity coefficient of Al is consistent with the experimental results, we can assume that the calculated activity of product species by Factsage is reliable.

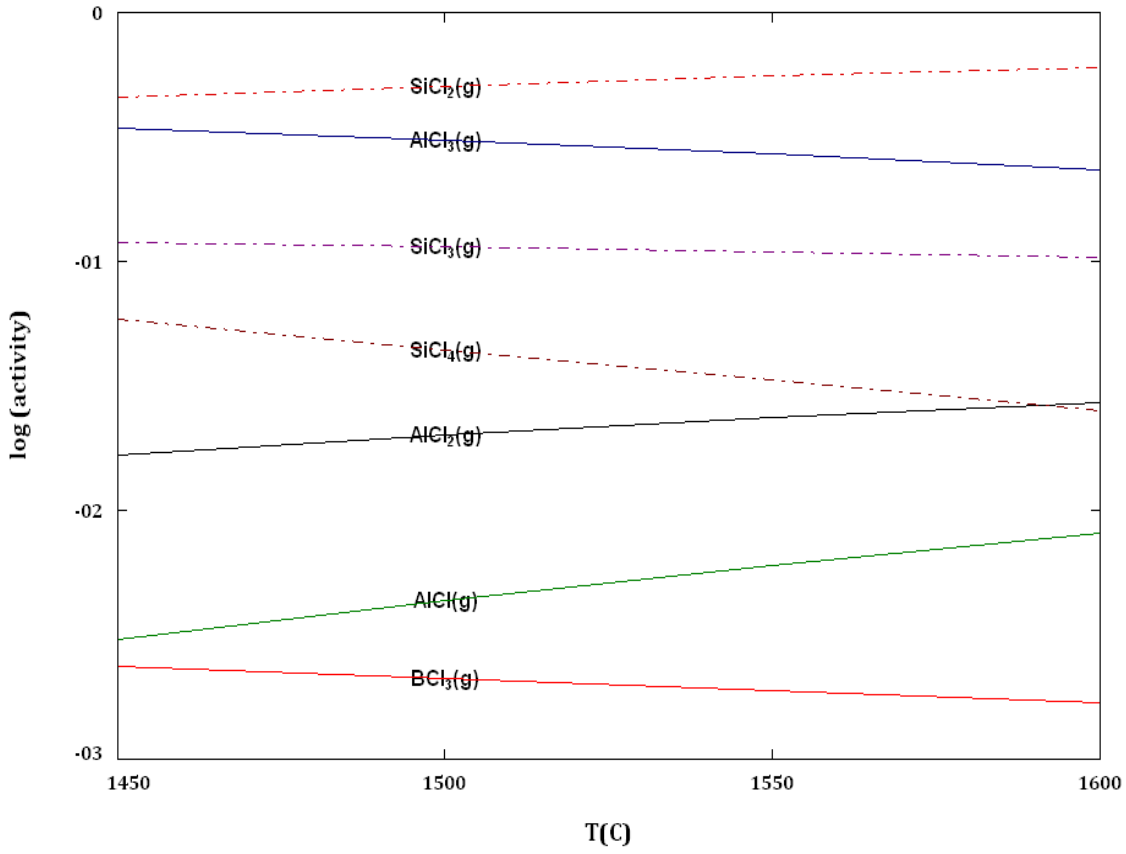


Figure 36: Activity of product species in chlorination process versus temperature
Reactants: Si (l) + 1E-3 Al (l) + 1E-5 B (l) + 1E-3 $SiCl_4$ (g)

The activity of the product species in the first step of chlorination is plotted versus temperature and shown in figure 36. The activity for the gas species below 1590°C decreases in the order $SiCl_2$> $AlCl_3$> $SiCl_3$> $SiCl_4$> $AlCl_2$> $BCl_3$> AlCl. In the next steps, $AlCl_3$

activity line lies below those of the silicon chloride species which is due to a decrease in Al concentration in the liquid silicon.

The boron and aluminum concentration level after the mentioned chlorination steps is shown in figure 37. As shown after four steps, boron and aluminum level is reduced to 0.5 ppmw and 0.25 ppmw, respectively. Calculations for each step show there is little loss in silicon content (0.06 %).

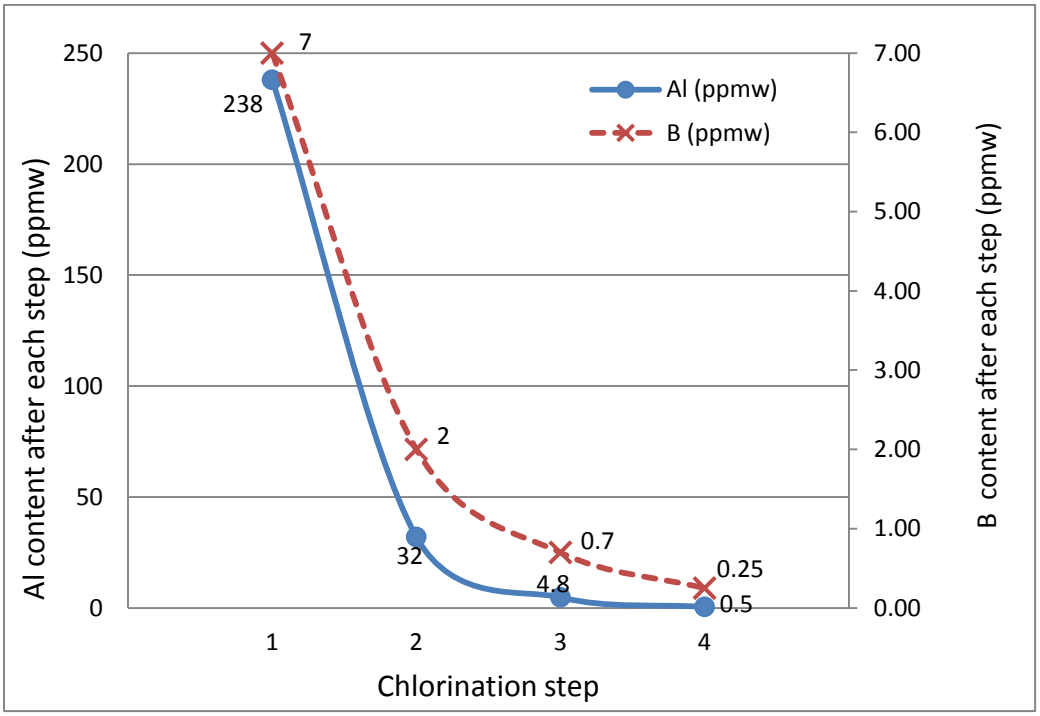


Figure 37: Aluminum and silicon decrease in multiple steps of the chlorination treatment calculated by Factsage

## 4.2. Al removal by chlorination process

In the experimental procedure of Al removal, two series of experiments were conducted. The first set was carried out using MG silicon with aluminum concentration level of 708 ppmw and boron level of 4.5 ppmw. In the second set, the silicon flakes used had a relatively high aluminum concentration of 3956 ppmw and low boron level of 0.44 ppmw. The chlorination treatment on the silicon flakes was aimed at aluminum removal.

### 4.2.1. Chlorination treatment on MG silicon

In the first series of experiments, the chlorination treatment was run on the MG silicon. The treatment temperature was set to 1450°C, the pressure was 1 atm and the treatment time was one hour. The reactant gas was Ar-0.33 vol% $SiCl_4$ with the flow rate of 200 mL/min and the silicon mass was about 35 gram. The result of ICP-OES analysis on MG silicon samples after the chlorination treatment at 1450°C is shown in figure 38. After one hour of chemical treatment, the Al content decreased to 154 ppmw by blowing and 45 ppmw by the injection method. The schematic showing the difference between blowing and injection methods was shown in figure 26. In the blowing method, the quartz tube which carries the reactant gas to the reaction zone was kept about 10 mm above the silicon melt, while in the injection method the quartz tube was inserted in the melt and positioned about 10 mm above the bottom and the reactant gas was

injected into the melt during the chlorination. When the treatment was completed, the quartz tube was gradually pulled out of the melt to prevent breakage of the tube when the liquid silicon solidified.

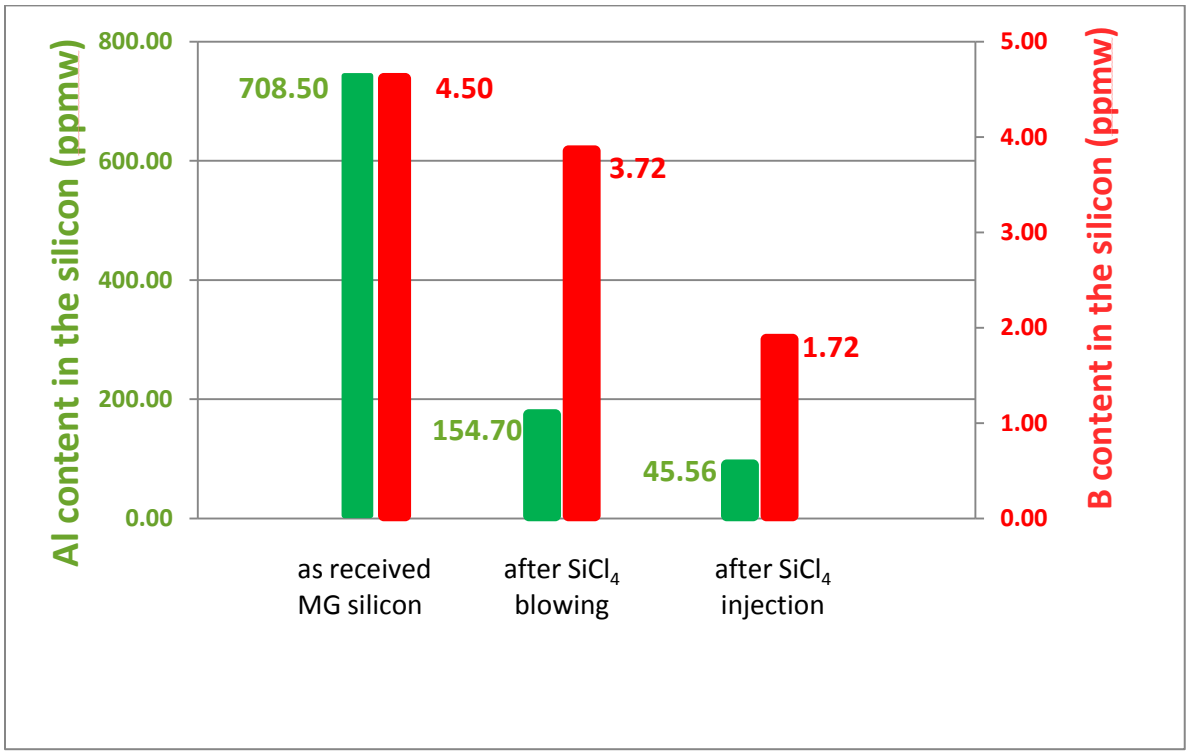


Figure 38: ICP-OES analysis after the chlorination process on MG silicon by blowing and injection method at 1450°C. (Gas flow rate of 200 mL/min)

Concentration of some other elements in MG silicon before and after chlorination is shown in Table 12. The chlorination process was not able to reduce the concentration of iron and titanium to any appreciable extent. This is attributed to low diffusivity of these impurities in liquid silicon.

Chlorination treatment by injection produced better results than blowing but in order to have better control of the process, the focus was on the blowing method. After injection, the results show that the boron level decreased to about one third of its initial content. The ICP analysis of the white yellowish powder product which was found on the tube walls revealed that the powder consisted of 35% silicon plus ppm traces of the other impurities. Therefore it seems the process involves the condensation of silicon, aluminum and boron compounds on the tube walls. The analysis of the powder product that condensed inside the chamber is included in table 12.

Table 12: Concentration of major elements before and after chlorination (ppmw)

| Elements | Before chlorination | After chlorination (blowing) | After chlorination (injection) | Powder Product of the chlorination (injection) |
|---|---|---|---|---|
| B | 4.50 | 3.72 | 1.72 | 2.97 |
| P | 49.57 | 41.19 | 46.95 | 27.45 |
| Al | 708.50 | 154.70 | 45.56 | 291.00 |
| Fe | 960.60 | 624.20 | 723.40 | 32.49 |
| Ti | 106.40 | 64.57 | 63.98 | <0.50 |

Boron could be only removed via formation of a compound at the reaction zone. Therefore there are two possible explanations for boron removal from silicon melt:

- Chlorination of boron, forming $BCl_3$
- Oxidation of B and evaporation of the products that condensed on the tube wall

The leakage test confirmed that the furnace is properly sealed, so the boron oxidation may not happen. In terms of thermodynamics regarding the chlorination of boron, as a simple calculation we can assume that the rate of removal is proportional to the partial pressure of the active species;

$$J_i \alpha P_i \qquad \text{Eq. 18}$$

where, $J_i$ and $P_i$ are removal rate and partial pressure of the component i. According to the calculations in table 10;

$$P_{(SiCl2)} \geq 200\ P_{(BCl3)} \qquad \text{Eq. 19}$$

$$J_{Si} \geq 200\ J_B \qquad \text{Eq. 20}$$

The boron removal rate can be calculated:

$$P_B = P^o_B\ a_B = P^o_B\ \gamma_B\ [B] \qquad \text{Eq. 21}$$

$$J_{Si} \alpha P_{Si} = 200\ P^o_B \qquad \text{Eq. 22}$$

$$J_B = (J_{Si}/200)\ \gamma_B\ [B] \qquad \text{Eq. 23}$$

where, $\gamma_B$ and [B] are the activity coefficient and the concentration of boron in the liquid silicon. Noguchi et al. [37] determined the activity coefficient of boron in the silicon melt by equilibrating solid BN and liquid Si in a nitrogen atmosphere from 1723 to 1923 K;

$$\mathrm{Log}\,\gamma_B = -\frac{1.11\times10^4}{T} + 5.82 \qquad [37] \qquad \text{Eq. 24}$$

Substituting the $\gamma_B$ value (~ 0.5 at 1450°C) from Eq. 24 in Eq. 23 and assuming the initial B level is 10 ppmw, and the silicon loss is 5% per hour,

$$J_B = 5 \times 0.5 \times 10^{-5}/200 = 1.25\times10^{-7}$$

$$\text{Boron removal fraction: } \frac{1.25\times10^{-7}}{10^{-5}} = \%\ 0.0125$$

Therefore, boron removal by chlorination treatment under the condition employed in the calculations seems not to be feasible although thermodynamically possible and a fraction of boron was removed in the process.

### 4.2.2. Chlorination treatment on the silicon flakes

The second set of experiments was done using the silicon flakes. In this set, the treatment temperature was 1475°C, the pressure 1 atm and the treatment time 60 min. The reactant gas, Ar-0.33 vol% $SiCl_4$, with the flow rate of 200 mL/min was blown to the surface of silicon flakes (35 gram) in an alumina crucible. The furnace atmosphere was protected with high purity argon gas with the flow rate of 300 mL/min. Sampling on the treated silicon was done when the furnace cooled down. The results of ICP analysis on the treated silicon flakes through blowing and injection methods are shown in figure 39. According to the graph, about 95% and 92% of initial aluminum in the silicon was removed by injection and blowing, respectively.

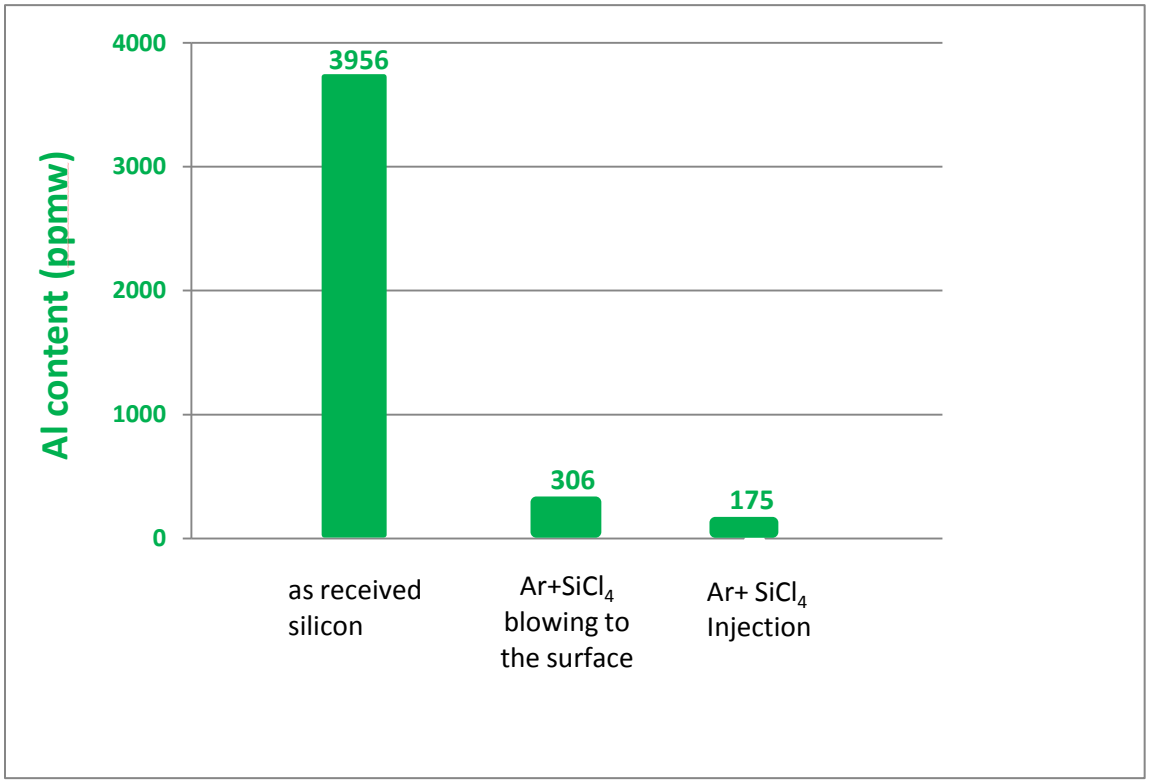


Figure 39: Effect of the chlorination process on Al removal in the silicon flakes (1475°C, 60 min)

High initial concentration of aluminum in the silicon flakes allowed a more accurate determination of the aluminum removal rate in the next step. The detection limit of the apparatus for ICP analysis was 1 ppmw and since the initial boron concentration in the silicon flakes was 0.44 ppmw, boron level change in the silicon flakes could not be measured in this set of experiments.

## 4.3. Determination of Al removal rate

To establish whether Al removal from silicon in the chlorination treatment was first order with respect to Al, the experimental data were fitted to Eq. 25, which is a first order rate equation;

$$\ln\left([Al]_t/[Al]_0\right) = -kt \qquad \text{Eq. 25}$$

$[Al]_t$: Concentration of Al at time t (ppmw)

$[Al]_0$: Initial concentration of Al (ppmw)

$k$: Apparent rate constant ($s^{-1}$)

If the rate of aluminum removal was zero order with respect to Al, then the rate of removal would be independent of any Al change in the silicon melt.

The Al concentration levels as a function of run duration in the chlorination treatment of MG silicon and its logarithmic plot are shown in figure 40 and figure 41. MG silicon with initial aluminum concentration of 1527 ppmw and boron concentration of 23 ppmw was chlorinated under the blowing method with the gas flow rate of 200 mL/min at 1450°C. Each point on the graph was obtained from separate experiments, and the sampling of treated silicon was done after the furnace cooled down. The linearity of the plot in figure 41 shows that the reaction is first order with respect to Al. The first order apparent rate constant, k= 0.0764 $sec^{-1}$, can be obtained from the slope of this plot.

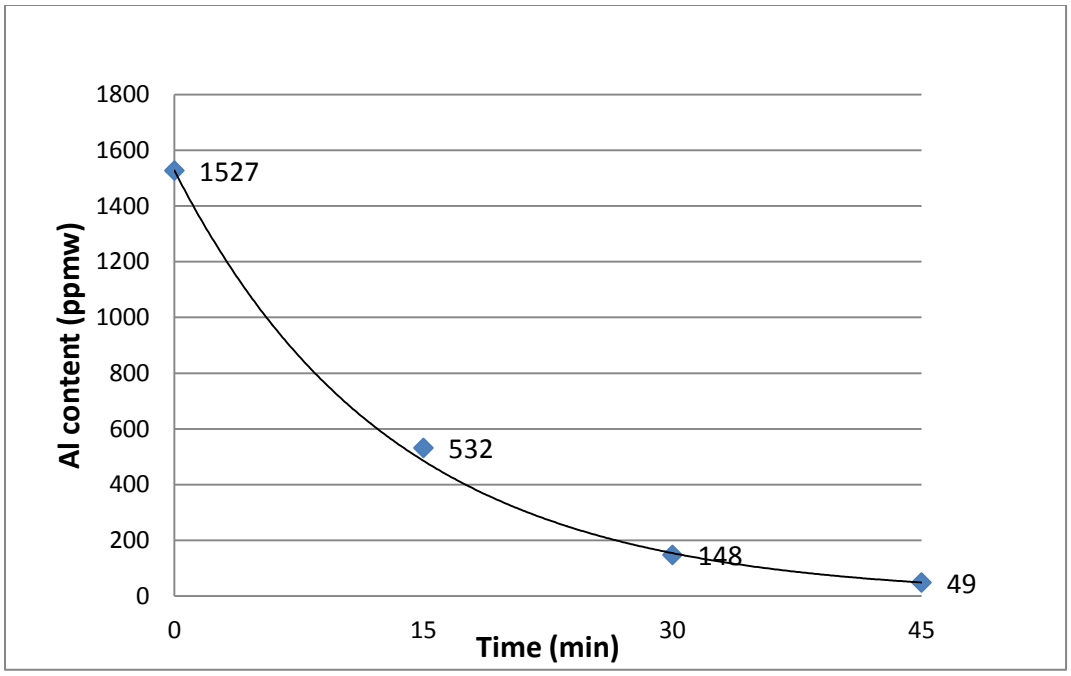


Figure 40: Aluminum removal rate in chlorination process of MG silicon by blowing method.

(T= 1450°C, Gas flow rate= 200 mL/min, P= 1 atm)

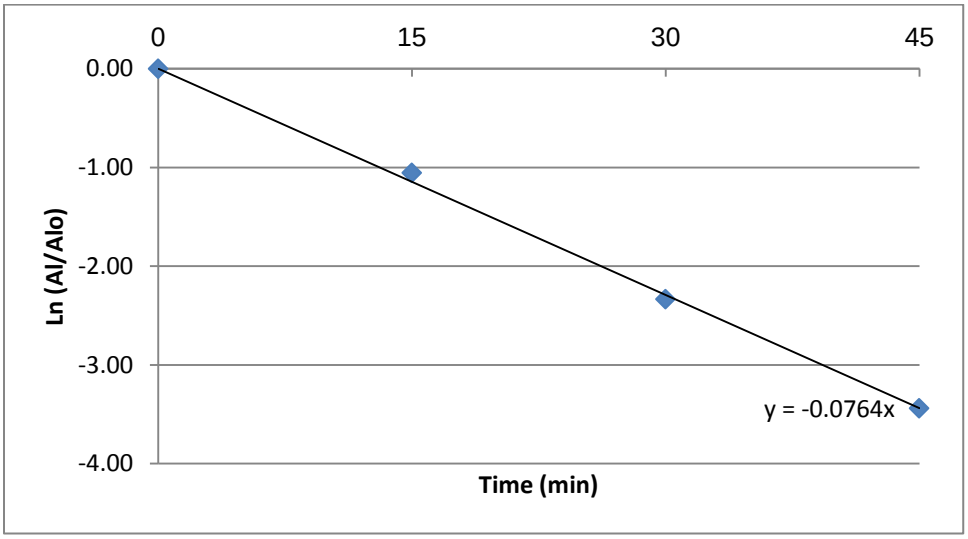


Figure 41: Logarithmic plot of Al removal rate in chlorination process of MG silicon

### 4.3.1. Rate determining step(s) in the Al removal

Knowledge of the rate determining step allows better control of the metallurgical process of impurity removal to be achieved. The rate determining step in a multistep reaction is one which is noticeably slower than the others. With Al removal in the chlorination treatment of MG silicon being a first order process with respect to Al, the possible rate determining step could be one or more of the following:

1. Transport of Al from the bulk to the reaction zone (surface of liquid silicon)
2. Chemical reaction between Al and $SiCl_4$
3. Transport of the products away from the reaction zone

In process metallurgy where high temperatures above the melting point of the metal are used, the chemical reaction is not usually the rate determining step and in most cases the transport of reactants to and/or products away from the reaction zone is the rate determining step [34]. The prediction was that the transport of Al from the bulk to the reaction zone is the rate determining step but the chemical reaction between Al and $SiCl_4$ was to be investigated as well.

The rate of mass transfer of aluminum in the bulk is given by Eq. 26;

$$J = k_M(C_{[Al]i} - C_{[Al]b}) \qquad \text{mol.cm}^{-2}.\text{s}^{-1} \qquad \text{Eq. 26}$$

where $k_M$ is a mass transfer coefficient and $[Al]i$ and $[Al]b$ denote the concentration of aluminum at the liquid silicon surface and in the bulk, respectively. When transport of Al from bulk to the liquid surface is the rate determining step, then the reaction of the

transferred Al with $SiCl_4$ at the liquid surface is at equilibrium during the removal process.

### 4.3.2. Effect of gas flow rate on the Al removal rate

A series of experiments was done to investigate the effect of flow rates of Ar+$SiCl_4$ gas on the removal of aluminum from melted silicon flakes. The effect of gas flow rate was tested at 100, 200 and 300 mL/min. The chlorination temperature was set at 1475°C for all the experiments. The graph of Al concentration levels versus the chlorination time at different gas flow rates is shown in figure 42.

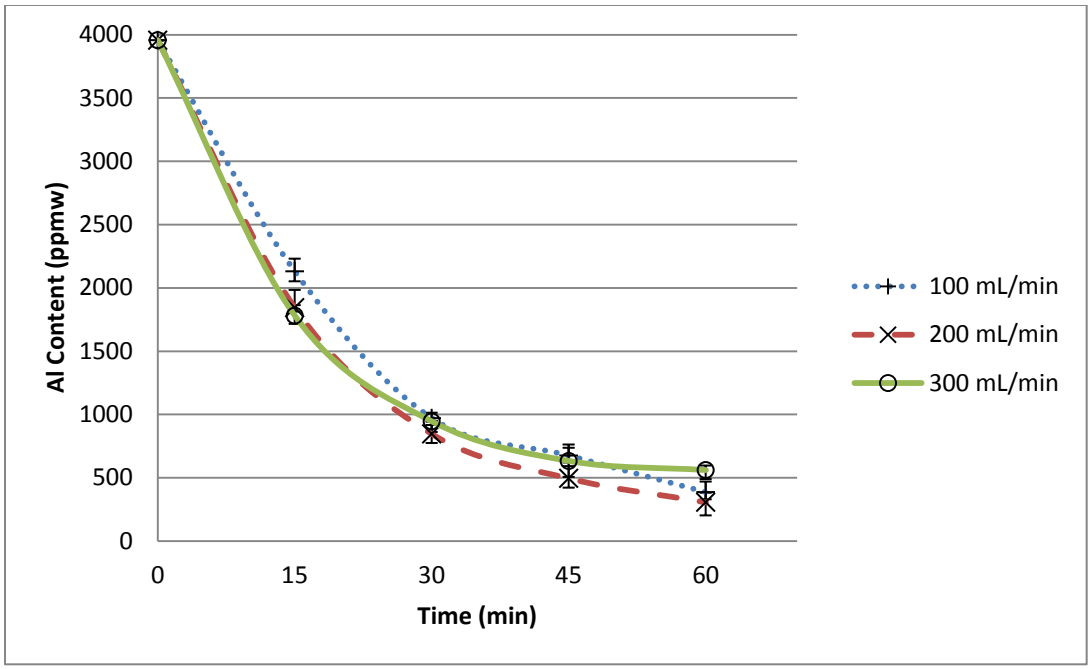


Figure 42: Al concentration levels versus the chlorination treatment time at different gas flow rates. (T= 1475°C, time= 60 min)

The graph in figure 42 was fitted using the equilibrium values at different gas flow rates and was plotted in logarithmic scale which is shown in fig 43. According to figure 42, it seems some of the points do not follow the trend of the removal rate. The reason could be related to the sampling condition. The sampling during the chlorination treatments were done consecutively in the intervals of 15 minute for each experimental run during which the $Ar+SiCl_4$ gas flow rate was stopped for a duration of about 20 sec. Since the sampling volume (1-2 $cm^3$) is subtracted from the silicon volume, after each sampling at 15 minute intervals, the volume from which Al is being removed decreases. Therefore, in order to get the best fit using the equilibrium values, only the first four points were taken to plot the fitted graphs in figure 42. It is seen that, at a gas flow rate of 100 mL/min, the removal rate of Al is the lowest. This is justified by considering the reactant gas transfer or product transfer to be the rate determining step. By increasing the gas flow rate from 100 to 200 mL/min, there is an increase in Al removal rate. There are two gas flow related causes of change. First, if due to gas starvation, then removal rate will be directly proportional to flow rate. Second, the gas phase mass transfer coefficient increases with flow rate which implies that there will be a more complex relation. Further increase of the gas flow rate to 300 mL/min did not improve the removal rate. This could be related to the mass transfer of Al in the metal being the rate determining step. Generally, by increasing the gas flow rate, the agitation of the liquid silicon would also increase. If we plot the rate constant versus the flow rate at 1475°C (figure 44), there is a changeover point at 200 mL/min flow rate. This changeover point indicates

that at this flow rate, the gas phase mass transfer is affected by another possible rate determining step, i.e., liquid phase mass transfer.

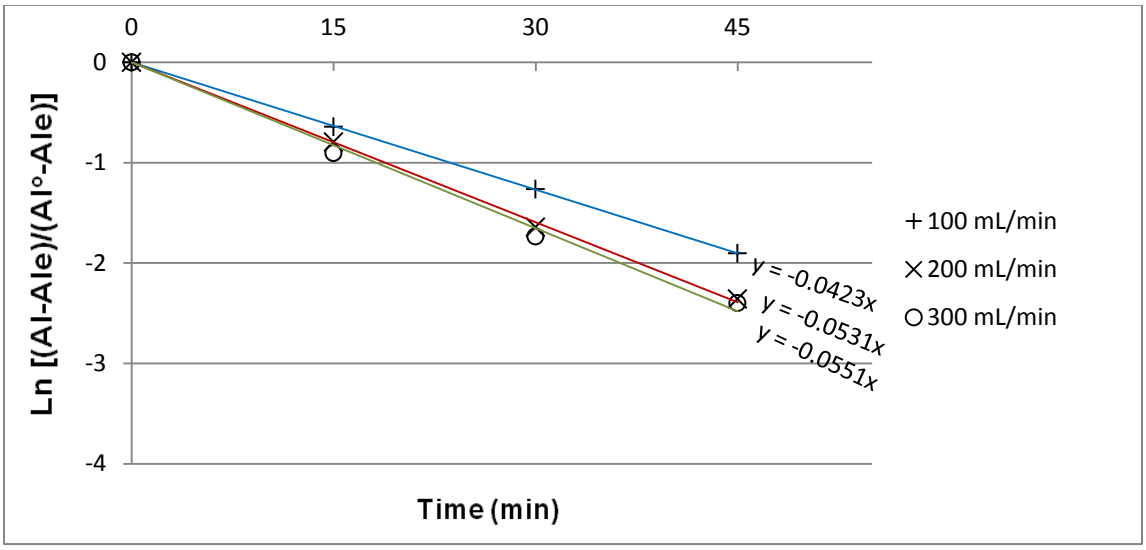


Figure 43: Logarithmic scale of Al removal rate in the chlorination treatment (blowing method) at 1475°C and different gas flow rates fitted using the equilibrium values

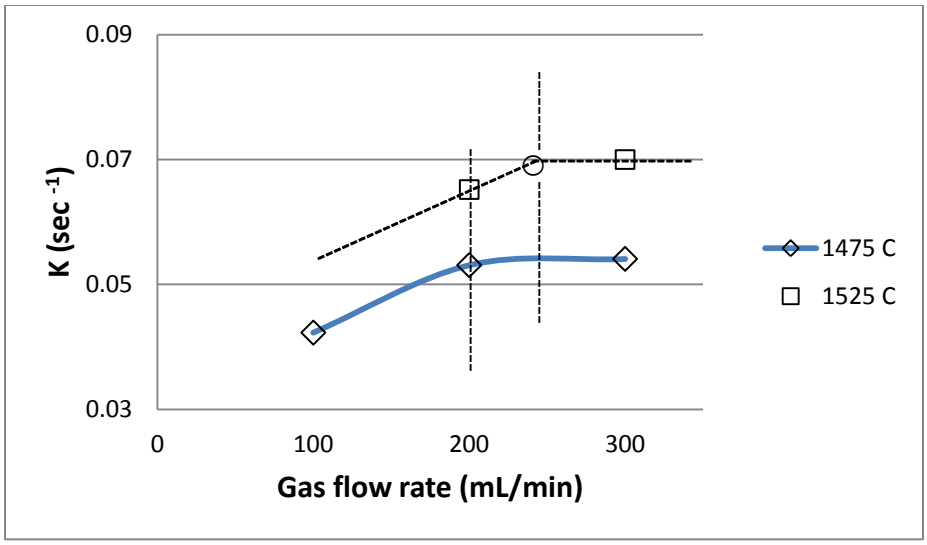


Figure 44: Al removal rate constant versus the flow rates in chlorination process of silicon flakes by blowing method at 1475°C and 1525°C.

In another series of experiments the flow rate of the gas was chosen to be 200 and 300 mL/min and the temperature was fixed at 1525°C. The Effect of Ar+SiCl4 flow rate on the Al removal rate in chlorination treatment is shown in figure 45. Equilibrium values at the interface were determined by fitting the data to the curves in figure 46. According to the graph, at gas flow rate of 300 mL/min, Al removal rate is close to that of 200 mL/min. This is attributed to the fact that by increasing the gas flow rate to 200 mL/min, the effect of gas phase mass transfer is eliminated and mass transfer of Al is the rate determining step. The rate constants obtained at 1525°C in figure 46 (the slopes of the lines) are also included in figure 44 for comparison with those of 1475°C. As seen in figure 44, by increasing the

temperature, the rate constant increases which is due to an increase in the liquid mass transfer rate. At higher temperature, this changeover point will move to higher flow rates in the graph (the probable changeover point is shown by the circle in figure 44). In other words, if we speed up the liquid phase mass transfer by increasing the temperature, the gas phase mass transfer would not change significantly. This is because of the temperature dependence of gas phase mass transfer and liquid phase mass transfer which are $T^{1.5}$ and exp T, respectively.

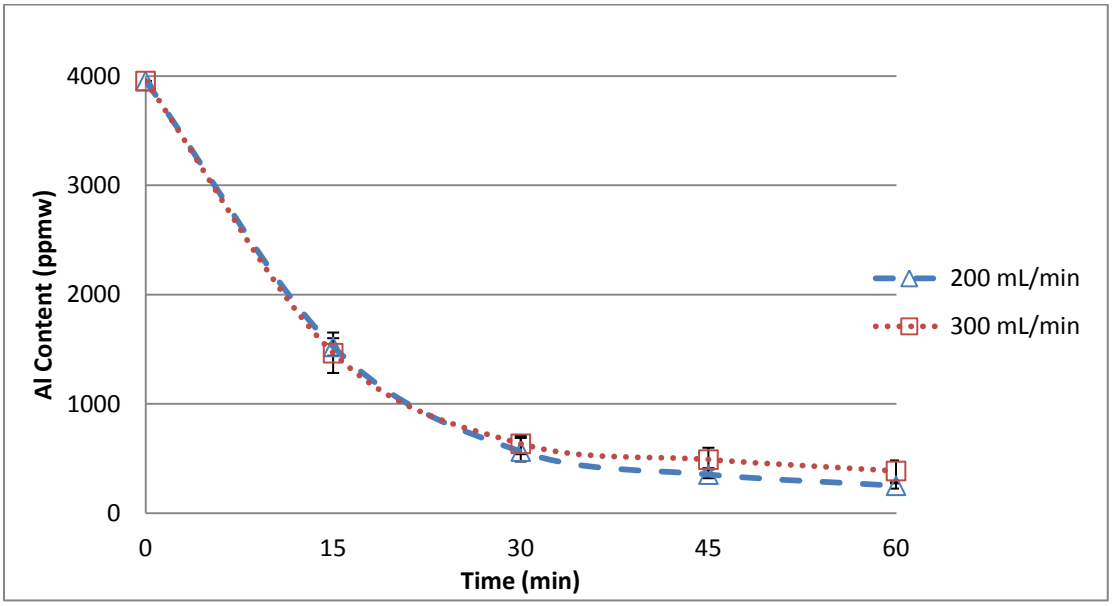


Figure 45: Effect of Ar+SiCl4 flow rate on the Al removal rate in chlorination treatment of silicon flakes (1525°C)

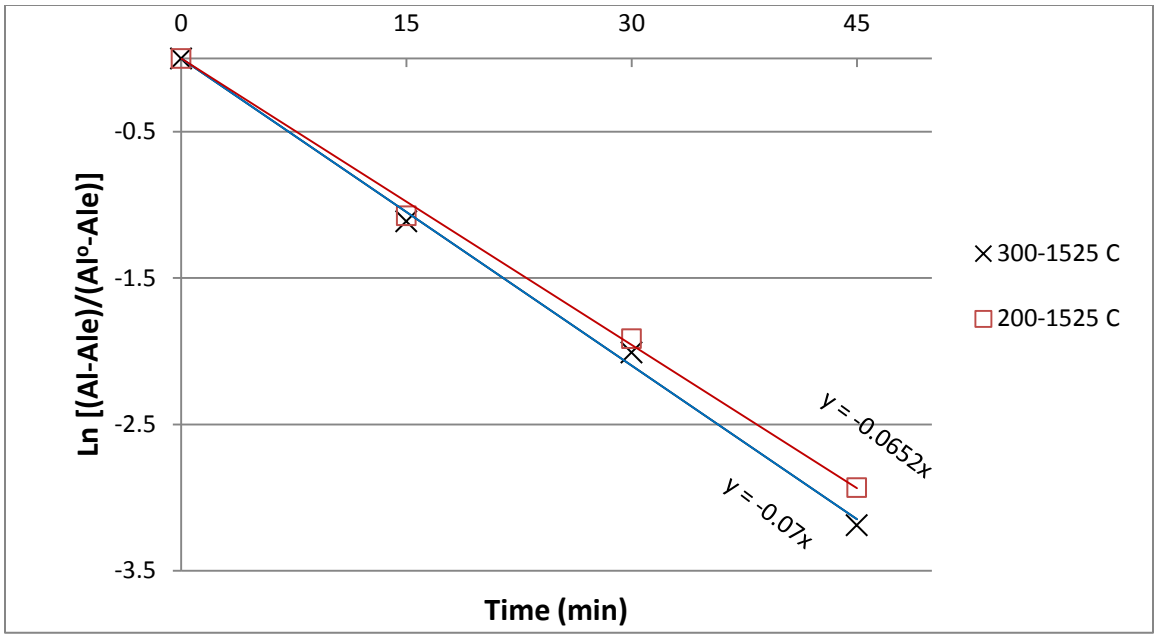


Figure 46: Logarithmic scale of Al removal rate in the chlorination treatment (blowing method) at 1525°C and gas flow rates of 200 and 300 mL/min fitted using the equilibrium values

In terms of thermodynamics, by considering the following simplified chlorination reaction:

$$SiCl_4 + 4/3\ Al = 4/3\ AlCl_3 + Si \qquad \text{Eq. 27}$$

The equilibrium constant is written as:

$$k_{eq.} = \frac{a_{Si}\ \ P_{AlCl3}^{4/3}}{[a_{Al}]^{4/3}\ P_{SiCl4}} \qquad \text{Eq. 28}$$

If the $SiCl_4$ gas flow rate was sufficiently slow for the liquid to maintain equilibrium with the gas, the removal rate would be totally dependent on the flow rate. In our case, we

have the opposite extreme. The gas flow is fast enough that we can assume a fixed gas composition and a fixed surface composition for the liquid silicon, and no rate dependency on flow.

### 4.3.3. Effect of Temperature on the Al removal rate

The mechanism of the liquid diffusion is not well established yet and the liquid impurity diffusion can still be described by the Arrhenius equation (Eq. 29);

$$D = D_o exp \frac{-E}{KT} \qquad \text{Eq. 29}$$

where $D_o$ and E, are pre-exponential factor and activation energy, k, Boltzmann constant and T is absolute temperature.

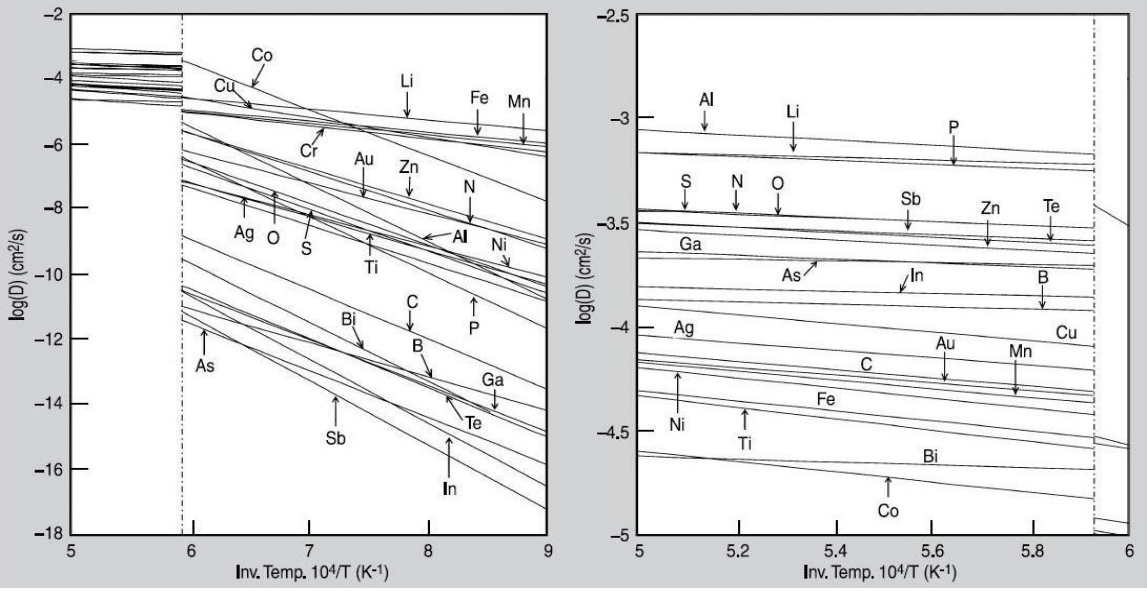


(a) (b)

Figure 47: The impurity diffusivities in solid silicon (a) The impurity diffusivities in liquid silicon (b) [60]

Based on the semi-empirical equations, the impurity diffusivities in solid and liquid silicon in the temperature range of practical interest, is shown in figure 47. The part (b) of this figure is the enlarged portion of part (a) for the impurity diffusivities in liquid silicon. Compared to other impurities in figure 47(b), the Al diffusivity line is at the top, indicating Al has the higher diffusivity in liquid silicon. As the temperature is increased, the average kinetic energy increases and the proportion of Al atoms greater than or equal to the activation energy of aluminum ($E_{Al}$= 24.1 kJ/mol [60]) also increases.

In another series of experiments, the effect of temperature on the Al removal rate of silicon flakes in the chlorination treatment was investigated. Effect of temperature on the removal rate at fixed flow rate of 200 mL/min is shown in figure 48. Equilibrium values at the interface then were determined by fitting the data to the curves in figure 49. The equilibrium values were obtained by extrapolation of the removal lines at each temperature. As seen in figure 49, by increasing temperature, the removal rate was increased. This can be attributed to an increase in the liquid mass transfer rate.

The equilibrium value doesn't matter early in the removal process but as aluminum concentration in the liquid decreases, i.e., the driving force becomes less ($\Delta C \downarrow$), equilibrium value starts to matter more, and deviation will happen. The crossover in figure 48 at 1500°C implies that the decreased stability of $AlCl_3$ results in a higher local $a_{Al}$ in equilibrium between the gas and the melt surface, and therefore the mass transfer rate will be slower. When the change of equilibrium is taken into account there is no cross over. All we can argue definitively is that by increasing temperature, as $AlCl_3$

becomes less stable, it is harder to remove Al at the interface, and hence the local equilibrium value for $a_{Al}$ will be higher and the removal rate might be reduced. In this case we have solved the problem of an unknown equilibrium value by fitting the kinetic equations for this value. Thus, by increasing temperature, it's thermodynamically harder to remove Al but kinetically more favorable. The obtained equilibrium values shown in figure 48 are consistent with the fact that by increasing temperature, the equilibrium values increase. In fact by fitting the curves using equilibrium values, the thermodynamic factor is removed.

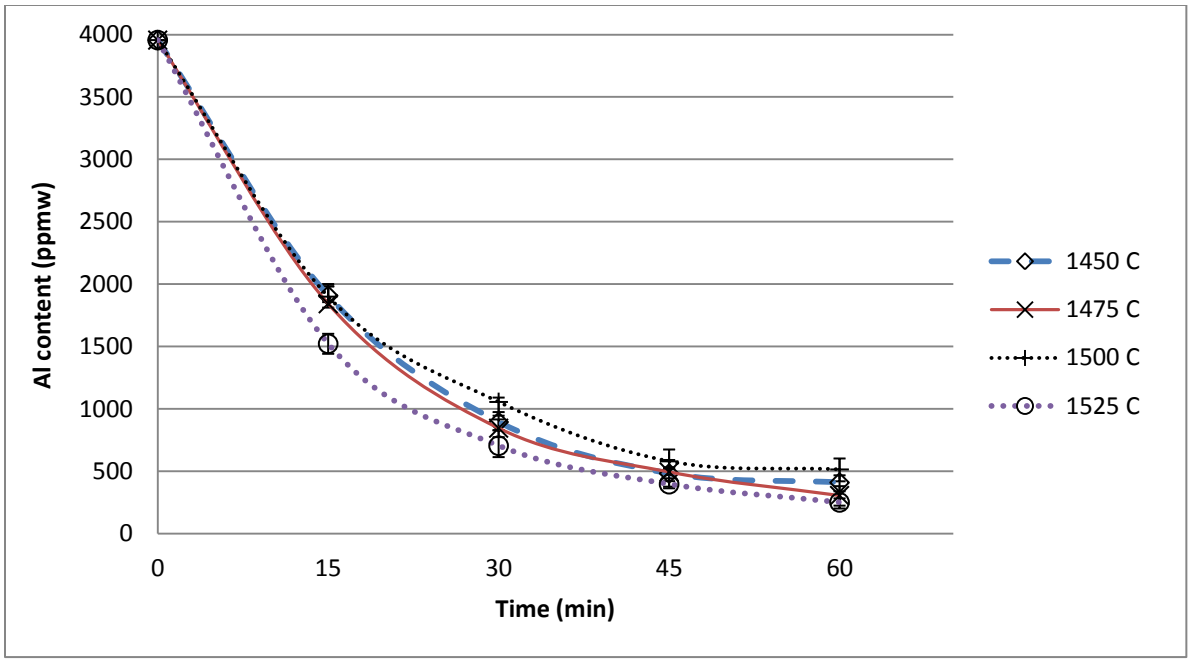


Figure 48: Effect of temperature on the Al removal rate (Ar+SiCl4 flow rate: 200 mL/min)

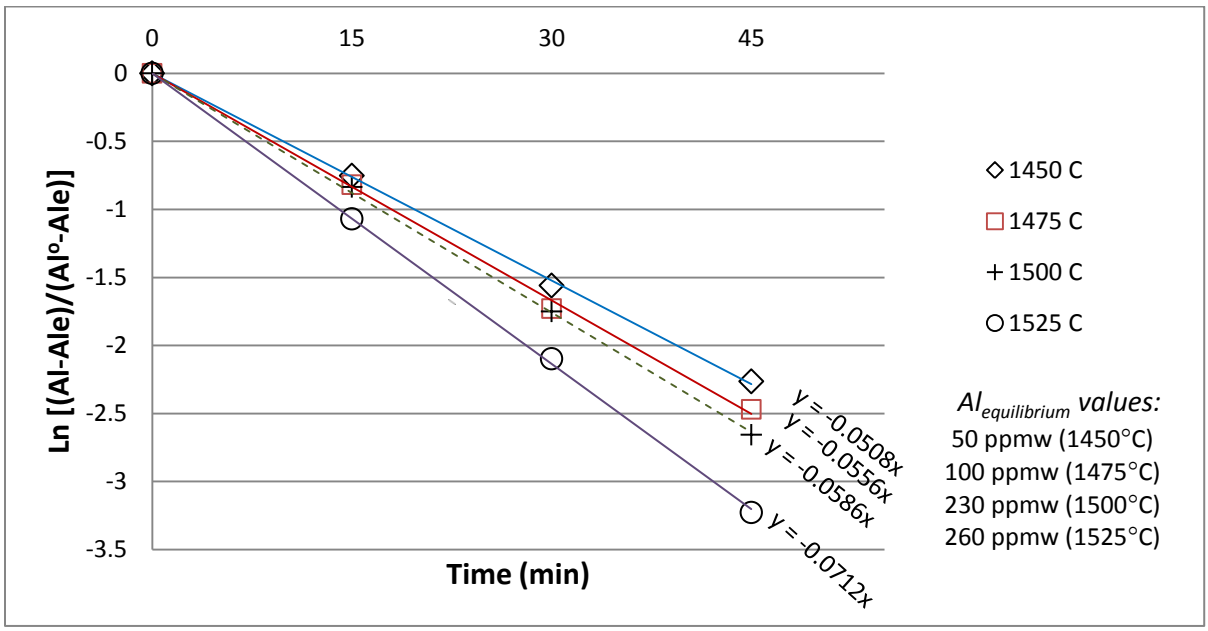


Figure 49: Logarithmic plot of Al removal rate in chlorination process of the silicon flakes at different temperatures and fixed flow rate of 200 mL/min (1 atm). Equilibrium values of Al could be obtained by either extrapolation of the removal curves in figure 48 or by getting the best straight lines in logarithmic scale

#### *4.3.3.1. Determination of activation energy*

The activation energy is a useful parameter in determining reaction mechanisms and in predicting reaction rates at given temperature. In order to obtain the activation energy, the values of k (the rate constant) at two different temperatures at least are required. By plotting Ln k versus 1/T, a straight line of slope –E/R is produced. The Arrhenius equation is given in Eq. 30;

$$k = A\ exp\frac{-E}{RT} \qquad \text{Eq. 30}$$

where A and E, are the pre-exponential factor and activation energy, R, gas constant and T is absolute temperature. The Arrhenius plot of Al removal at different chlorination temperatures and fixed flow rate of 200 mL/min is shown in figure 50.

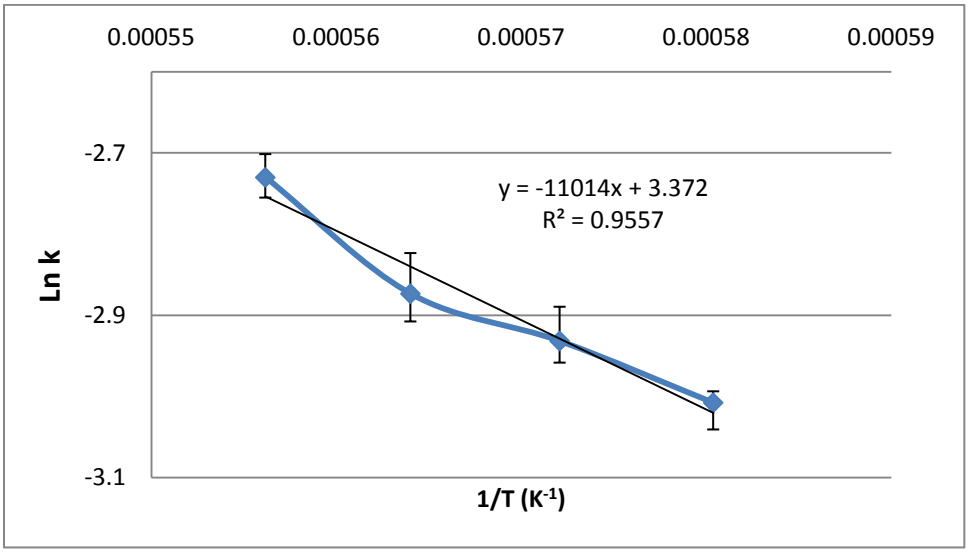


Figure 50: Arrhenius plot of Al removal at different chlorination temperatures and fixed flow rate of 200 mL/min

In order to check the accuracy of the fitted graph in figure 49, the range of equilibrium values that give the best fit at each temperature was obtained and the error bars in figure 50 were produced.

Normally when we talk in terms of rate determining step (RDS), we consider consecutive reaction steps, the slowest of which will control the rate. According to figure 50, it appears there may be a change in rate determining step at 1500°C. As shown schematically in figure 51, if there is a mechanism change between step 1 and step 2, there may be a parallel step, because the faster step is RDS. There is no obvious basis for parallel steps in this reaction system. Therefore, the deviation in the graph should be considered to arise from scatter in the data.

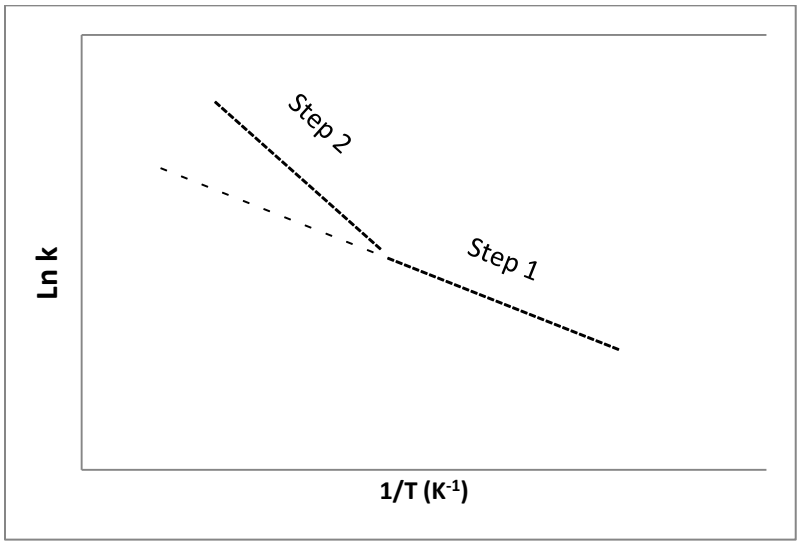


Figure 51: Schematic of Arrhenius plot for a reaction with consecutive mechanisms including step 1 and step 2

### 4.3.4. Blowing versus injection method

As stated earlier, blowing and injection were two methods used for chlorination of silicon in this study. The injection of different gases into liquid metal is a well known method of many refining treatments. The size of bubbles has an important role in determining the chemical kinetics as well as mass transfer during the process. Bubble formation is known to be a very complicated phenomenon because different variables (gas flow rate, nozzle diameter, liquid and gas properties,…) are involved. At low gas flow rates, bubble formation at the tip of the nozzle is essentially determined by surface phenomena. Li et al. [61] investigated wetting of ceramic materials by liquid silicon. According to their work, the contact angle of liquid silicon on an alumina tube as used for Ar+$SiCl_4$ injection in our study is 80° (figure 52).

According to figure 52, the contact angle of silicon/ceramic systems is closely related to the band gap energy of ceramics. This indicates the existence of localized chemical bonds at the interface between silicon and a non-metallic solid ceramic, which is due to the electron transfer at the silicon/ceramic interface. [61]

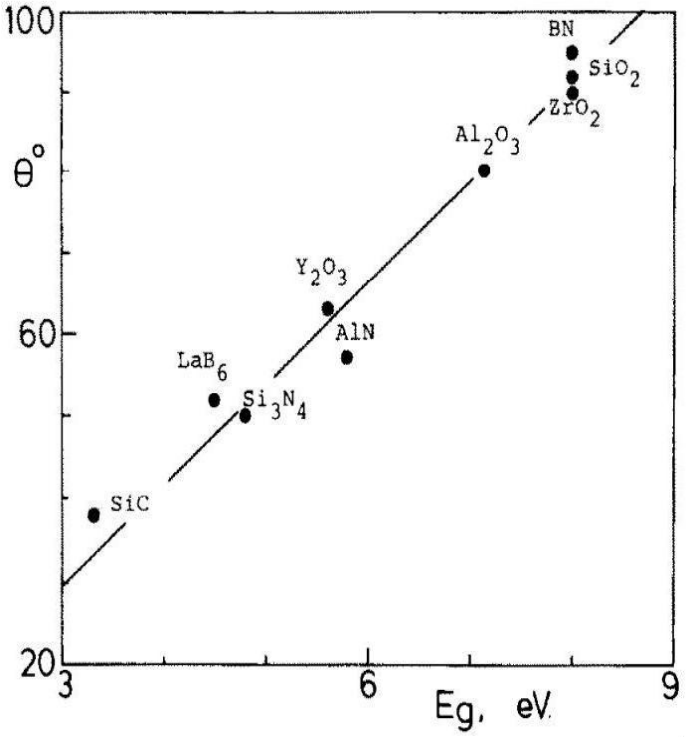


Figure 52: Contact angle θ of liquid silicon on various solid ceramics as a function of the band gap energy Eg of the ceramics. [61]

Therefore, silicon is wetting the alumina surface and the bubble size, $V_b$, at release from nozzle with inner diameter of $D_i$ is given by

$$V_b = \pi D_i \sigma / (\rho - \rho_g)g \qquad [62] \qquad \text{Eq. 31}$$

where $\rho$ and $\rho_g$ the densities of liquid and gas, respectively, σ the surface tension of the liquid-gas interface, g the acceleration due to gravity. Millot et al. [63] studied the

surface tension of liquid silicon at high temperature and presented the following relation;

$$\sigma = (732 \pm 8) - (0.086 \pm 0.004)(T - 1685) \quad \text{Eq. 32}$$

With $\sigma$ in mN/m, and temperature in K, the surface tension value of liquid silicon at 1475°C was calculated in the range of

$$\sigma = 720.3 - 736.3 \text{ mN/m (or dyne/cm)}$$

Then, considering $D_i$= 0.6 cm, ρ ($Si_l$) = 2.57 g/cm$^3$, $\rho_g$= 1.2 × 10$^{-3}$ g/cm$^3$, the bubble size was calculated in the range of $V_b$= 0.54–0.55 cm$^3$ which gives the surface area range of $A_b$= 3.21–3.25 cm$^2$ for each bubble.

Bubble size and equivalent diameter as a function of flow rate, at the bath temperature in metallic systems is shown in figure 53. As seen, at low flow rates, the bubble size remains unchanged independently of moderate changes in the gas flow rate. Thus, as the gas flow rate is increased, bubbles of the same size form with increasing frequency. As the gas flow rate further increases the bubble frequency levels off at a constant value and thereafter the bubble size increases proportionally to the gas flow rate until a continuous jet occurs. [64, 65].

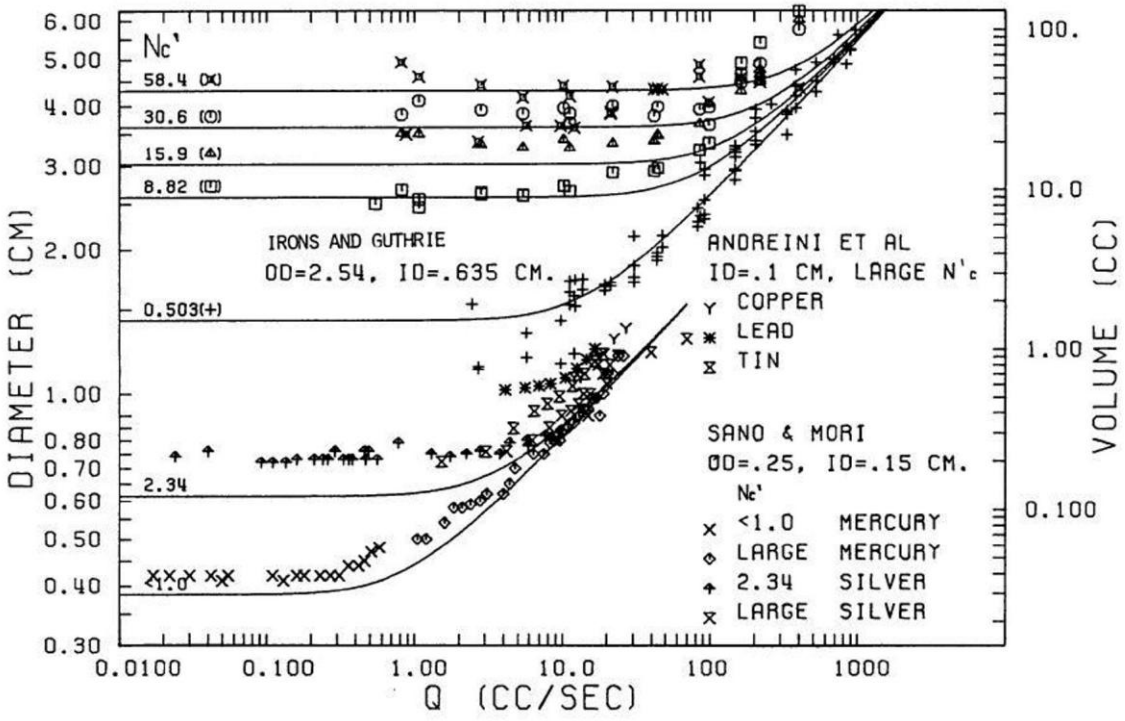


Figure 53: Bubble size and equivalent diameter as a function of flow rate, at the bath temperature in metallic systems. (N'c is the chamber volume effect) [64]

A comparison of the blowing and injection methods in Al removal of the silicon flakes is shown in figure 54. No sampling was done for the injection method during the chlorination and only the end point was used for this comparison. It should be noted that the equilibrium value for the injection condition can't be higher than the value for blowing. Therefore, the rate constant for injection was obtained using the same equilibrium value for blowing, $Al_e$ (1475°C) = 100 ppmw.

As seen in figure 54, the removal rate is higher for the injection condition. The difference in the apparent rate constant has two origins:

1. The liquid is stirred faster by injection and the mass transfer rate increases.

2. The ratio of area/volume (S/V) increases.

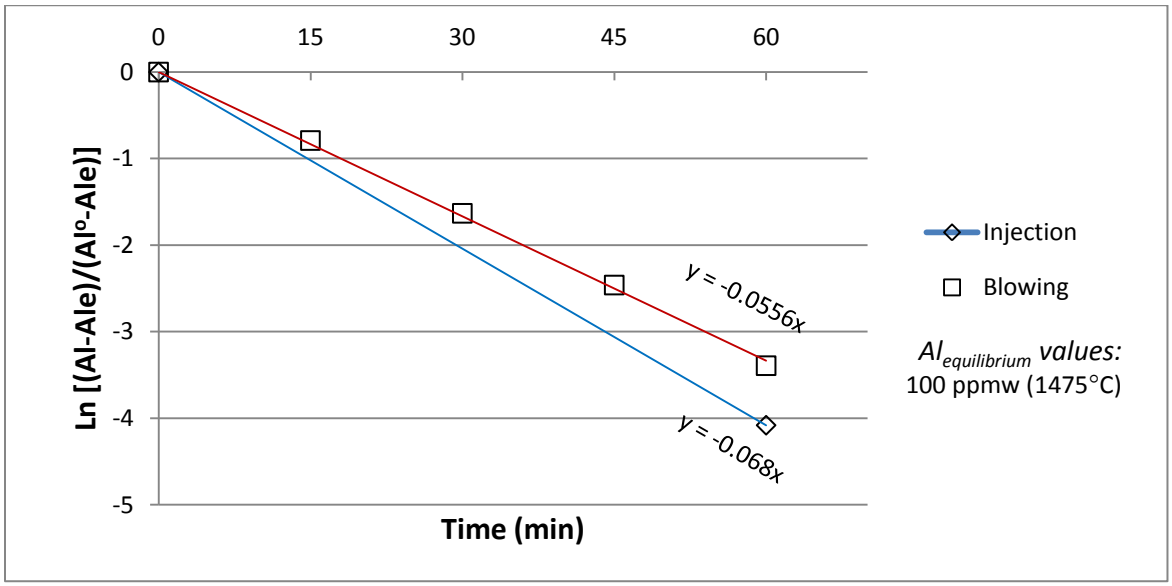


Figure 54: Al removal rate in chlorination of silicon flakes by two separate methods: blowing and injection (T: 1475°C, gas flow rate: 200 mL/min, time: 60 min)

If we calculate the total surface area which is created by forming bubbles in the liquid, we can determine the extent to which stirring and an increase of surface area contribute to the increase in rate for injection.

For a bubble rising in infinite media it's possible to prepare a generalized graphical correlation in terms of the Eotvos number (Eo), Morton number (Mo) and Reynolds number (Re); [66]

$$Eo = g \rho D_b^2 / \sigma \qquad \text{Eq. 33}$$

$$M = g \mu^4 / \rho \sigma^3 \qquad \text{Eq. 34}$$

$$Re = \rho D_b U / \mu \qquad \text{Eq. 35}$$

where g is gravitational acceleration, $D_b$ is bubble sphere equivalent diameter, $\mu$ is viscosity of liquid and U is the velocity of bubbles. The resulting plot is shown in figure 54.

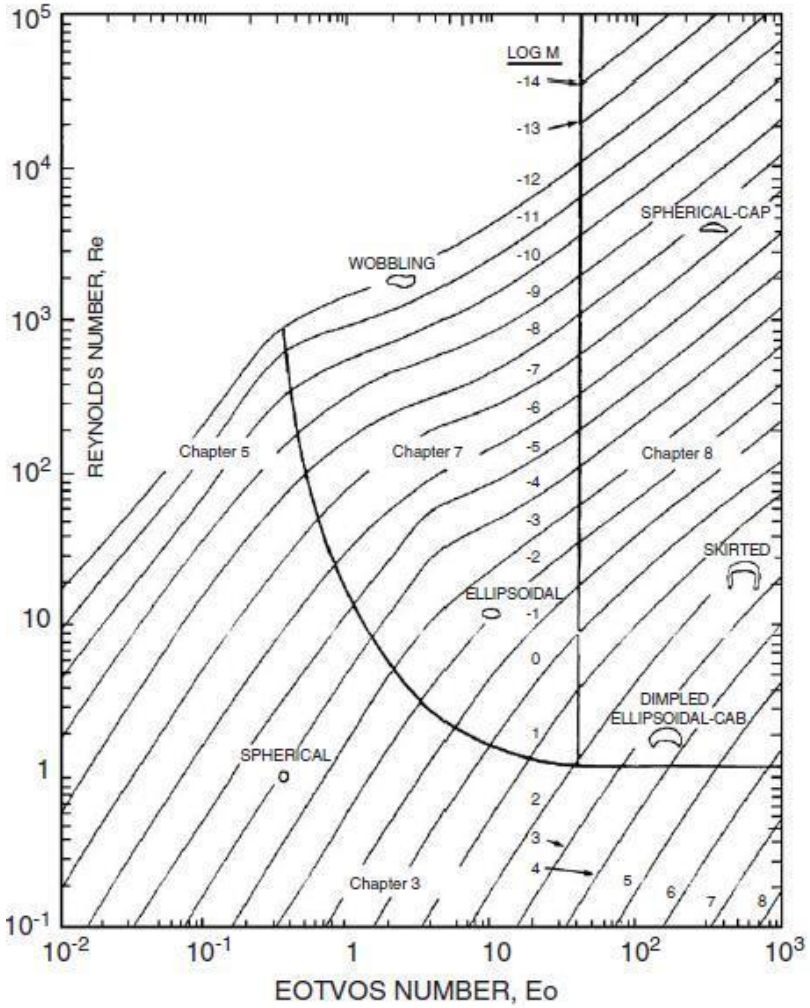


Figure 55: Shape regime for bubbles in unhindered gravitational motion through liquids [65]

By correlating the mentioned numbers, the velocity of bubbles, U was calculated 2.52 cm/sec. The total surface area due to bubbling can be obtained as:

instant number of bubbles= rate of bubble generation × residence time

$$= 6.17 \text{ (bubbles/sec)} \times 0.39 \text{ (sec)} = 2.45$$

Since the effective surface area is provided by instant complete bubbles, thus the bubble number (n) will be equal to 2.

total surface area (A) = n × surface area of each bubble ($A_b$)

$A = 2 \times 3.23 \text{ (cm}^2\text{)} = 6.46 \text{ cm}^2$

The surface area in blowing condition was calculated as 8.04 $cm^2$. Since the total surface area in the injection condition is less than that of blowing, then stirring of the melt by gas injection improves the mass transport in the liquid and is the main reason for higher removal rate.

### 4.3.5. Kinetics of boron removal

The boron removal work of Tang et al. [59] through $H_2$-$H_2O$ mixture is converted to a logarithmic scale and shown in figure 56. The graph is also fitted for the equilibrium values which were found to be 0.7 and 3 ppmw at 1450°C and 1500°C respectively. The initial boron level for their experiments was 50 ppmw and the gas flow rate was 3 L/min. They reported the boron removal at low temperatures occurred at a faster rate and the chemical reaction was the rate controlling step. Since the removal rate is proportional to the vapor pressure of boron hydroxide species and on the other hand major product

species (e.g. $B_3H_3O_3$) are less stable at higher temperatures, we believe either chemical reaction or gas phase mass transfer could be the rate determining step in their boron removal process. The boron removal through blowing and injection method in MG silicon (from figure 39) is also included in figure 55. Regarding the boron removal in the chlorination treatment by blowing and injection, the rate is considerably faster in the injection. Stepwise suggest this should not be feasible in the time available thermodynamic calculations suggest that B removal at the level observed is possible. However, analyses of the kinetics relative to the rate of Si loss suggest that this is not feasible. The author is not able to offer an explanation for the conflict between analysis and experimental observation however, since the rate is much faster in the injection condition, the rate is likely to be controlled by mass transport in the liquid.

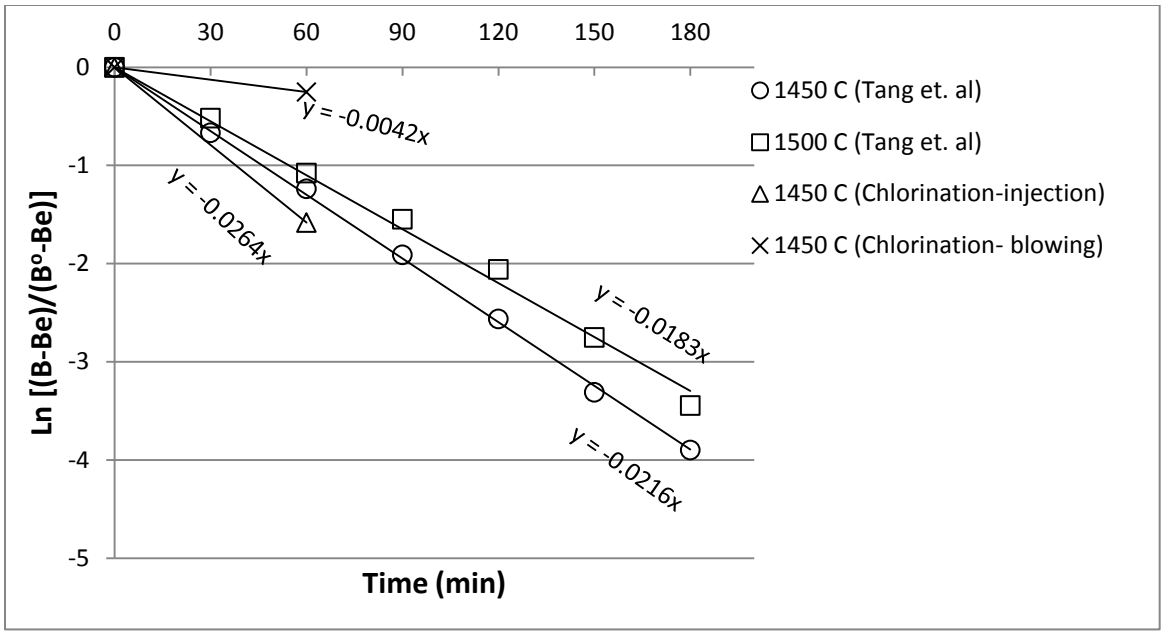


Figure 56: Boron removal rate in chlorination treatment of MG silicon by blowing and injection. The results are compared with the results of Tang et al. [59] for boron removal by hydrogen water vapor gas mixture.

Regarding the boron removal by different gas mixtures reviewed in chapter 2; oxygen and oxygen water vapor (Wu et al. [33]), hydrogen water vapor (Tang et al. [59]) and water vapor gas combined with directional solidification (Khattak et al. [5]), the feasibility of boron removal was reported but the efficiency and reproducibility of the removal was not confirmed.

# 5. Summary and Conclusion

In this research, refining of metallurgical grade silicon by chlorination treatment with the emphasis on Al removal was investigated. Thermodynamic calculations through Factsage confirmed the feasibility of Al removal in repeated steps of chlorination. Therefore, an Ar+$SiCl_4$ gas mixture was applied to the silicon melt by blowing and injection methods and the ICP-OES was used for analysis of the impurities in silicon. The main results found for this research are summarized as:

- Al was removed in the chlorination treatment mainly in the form of $AlCl_3$. As chlorination proceeds and Al concentration decreases in the liquid silicon, the fraction of $AlCl_3$ in the gas product phase decreases. Conversely, the share of silicon chloride species increases.
- In chlorination treatment, the activity for the gas species below 1590°C decreases in the order $SiCl_2$> $AlCl_3$> $SiCl_3$> $SiCl_4$> $AlCl_2$> $BCl_3$> AlCl.
- Thermodynamic calculations suggest that B removal at the level observed is possible. However, analyses of the kinetics relative to the rate of silicon loss suggest that this is not feasible. The author is not able to offer an explanation for the conflict between analysis and experimental observation.
- Al removal from silicon by chlorination treatment under the conditions employed in this study is first order reaction with respect to Al.

- By increasing the temperature in the chlorination process, the liquid phase mass transfer coefficient increases which controls the removal rate.
- At higher temperatures $AlCl_3$ is relatively less stable therefore the Al activity in local equilibrium at the surface will become higher which will impede the mass transport rate. This effect resulted in the observed maximum in Al removal rates at intermediate temperatures. When the local equilibrium at the metal surface was accounted for in the kinetic analysis a monotonic increase in apparent rate constant (mass transfer coefficient) with temperature was observed.
- The observed higher rates of Al removal under injection conditions appear to be the result of improved stirring in the melt rather than an increase in the interfacial area.

## 7. References

1. US Department of Energy, National renewable energy laboratory, Photovoltaics energy for the new millennium, The National 2000–2004 Photovoltaics Program Plan, January 2000

2. Flamanta et al, "Purification of metallurgical grade silicon by solar process", Sol Energy Matter Solar Cells (2006) 90:2099-2106

3. Yuge et al, "Purification of metallurgical grade silicon up to solar grade", Sol Energy Matter Solar Cells (1994) 34:243-250

4. Ciszek et al, "Alternative Solar-Grade Silicon Feedstock Approaches", NCPV Program Rev. Meet., (2001) Lakewood, Colorado

5. Khattak et al, " A simple process to remove boron from Metallurgical grade silicon", Solar Energy Materials & Solar Cells 74 (2002) 77–89

6. Ikeda et al, "Purification of silicon for solar-grade silicon by electron beam metallurgical button melting", ISIJ Int (1992) 32:635-642

7. Yu et al, "Removal of iron and aluminum impurities from metallurgical grade silicon with hydrometallurgical route", Trans Nonferrous Met Soc China (2007) 17:1022-1025

8. Gribov et al, "Preparation of high purity silicon for solar cells", Inorg Matter (2003) 39:653-662

9. S. Pizzini, Sol. Energy Mater. 6 (1982) 253

10. T.F. Ciszek, T.H.Wang, M.R. Page, R.E. Bauer, M.D. Landry, Conference Record of the 29th IEEE Photovoltaic Specialists Conference 2002 (Cat. No.02CH37361), IEEE, Piscataway, NJ, USA, 2002, p. 206

11. W.C. Breneman, E.G. Farrier, H. Morihara, 13th IEEE Photovoltaic Specialists Conference, IEEE, New York, NY, USA, 1978, pp. 339–343

12. M.F. Browning, J.M. Blocher Jr.,W.J.Wilson, D.C. Carmichael, 12th IEEE Photovoltaic Specialists Conference, IEEE, NewYork,NY, USA, 1976, pp. 130–136

13. B.R. Bathey, M.C. Cretella, “"Review Solar-Grade Silicon", J. Mater. Sci. 17 (1982) 3077

14. W.V. Gampel, US Patent 2,972,521 (1961)

15. E. Bildl, J. Dietl, R. Baueregger, D. Seifert, US Patent 4,588,571 (1984)

16. C.E. Norman, E.M. Absi, R.E. Thomas, Can. J. Phys. 63 (1985) 859

17. L.P. Hunt, V.D. Dosaj, J.R. McCormick, L.D. Crossman, 12th IEEE Photovoltaic Specialists Conference, IEEE, New York, NY, USA, 1976, pp.125–129.

18. E. Bildl, J. Dietl, R. Baueregger, D. Seifert, US Patent 4,588,571 (1984)

19. Morita et al, "Thermodynamics of solar-grade silicon refining", Intermetallics 11 (2003) 1111-1117

20. S. Tsao et al., Mater. Sci. Forum 475–479 (2005) 2595.

21. N. Yuge, H. Baba, Y. Sakaguchi, K. Nishikawa, H. Terashima, F. Aratani, Sol. Energy Mater. Sol. Cells 34 (1994) 243

22. N. Yuge, M. Abe, K. Hanazawa, H. Baba, N. Nakamura, Y. Kato, Y. Sakaguchi, S. Hiwasa, F. Aratani, Prog. Photovoltaics Res. Appl. 9 (2001) 203

23. D. Morvan, I. Cazard-Juvernat, J. Amouroux, J. Mater. Res. 13 (1998) 2709

24. C. Alemany, C. Trassy, B. Pateyron, K.I. Li, Y. Delannoy, Sol. Energy Mater. Sol. Cells 72 (2002) 41

25. Y. Delannoy, C. Alemany, K.I. Li, P. Proulx, C. Trassy, Sol. Energy Mater. Sol. Cells 72 (2002) 69

26. N. Nakamura, H. Baba, Y. Sakaguchi, Y. Kato, Mater. Trans. 45 (2004) 858

27. N. Nakamura, H. Baba, Y. Sakaguchi, S. Hiwasa, Y. Kato, J. Jpn. Inst. Met. 67 (2003) 583

28. K. Hanazawa, N. Yuge, Y. Kato, Mater. Trans. 45 (2004) 844

29. K. Hanazawa, N. Yuge, S. Hiwasa, Y. Kato, J. Jpn. Inst. Met. 67 (2003) 569

30. T.L. Chu, G.A. van der Leeden, H.I. Yoo, "Purification and Characterization of Metallurgical Silicon", J. Electrochem. Soc. 125 (1978) 661

31. C.P. Khattak, D.B. Joyce, F. Schmid, Conference Record of the 29th IEEE Photovoltaic Specialists Conference 2002, IEEE, Piscataway, NJ, USA, 2002, p. 364

32. H.C. Theuerer, "Removal of Boron from Silicon by Hydrogen Water Vapor Treatment", J. Metals, 8 (1956), pp. 1316–1319.

33. Ji-jun et al, "Boron removal from metallurgical grade silicon by oxidizing refining", Trans. Nonferrous Met. Soc. China 19 (2009) 463-467

34. J.J. Moore, “Chemical Metallurgy”, 2nd edition, Butterworthes, 1990

35. L.A.V. Teixeira and K. Morita, "Removal of Boron from molten silicon using CaO-SiO2 based slags", ISIJ International, Vol. 49 (2009) No. 6, pp. 783-787

36. Teixeira et al, "Behavior and state of boron in CaO-SiO2 slags during refining of solar grade silicon", ISIJ (2009) pp. 777-782

37. Noguchi et al, "Thermodynamics of Boron in a Silicon Melt", Metallurgical and Materials Transaction B, (1994) Vol. 25B pp. 903-907

38. Zaitsev et al, "Thermodynamic Properties of CaF2+ SiO2+ CaO Melts", Inorganic Materials, Vol. 33, No.1, 1997, pp. 68-77

39. T. Yoshikawa and K. Morita, "Thermodynamic Property of B in Molten Si and Phase Relations", Mater. Trans., 46 (2005), p. 1335-1340

40. J.A. Duffy, "A review of optical basicity and its applications to oxidic systems", Geochimica et Cosmochimica Acta Vol. 57 Issue 16 (1993) Pages 3961-3970

41. C.P. Khattak, D.B. Joyce, F. Schmid, Conference Record of the 29th IEEE Photovoltaic Specialists Conference 2002, IEEE, Piscataway, NJ, USA, 2002, p. 364

42. Yoshikawa, K. Arimura and K. Morita, Metalurgical and Materials Transactions B, Vol. 36B (2005) 837-842

43. T. Yoshikawa and K. Morita: J. Electrochem. Soc. (2003) vol. 150, pp. G465-G468

44. T. Yoshikawa and K. Morita: Sci. Technol. Adv. Mater. (2003) vol. 4, pp. 531-37

45. T. Yoshikawa and K. Morita: J. Phys. Chem. Solids (2005) vol. 66, pp. 261-65

46. T. Yoshikawa and K. Morita: Proc. 2005 TMS Annual Meeting, Extraction and Processing Division, San Francisco, CA, 2005, TMS, Warrendale, PA (2005) pp. 549-558

47. T. Yoshikawa and K. Morita: Iron Steel Inst. Jpn. Int. (2005) pp. 967-71

48. T. Yoshikawa and K. Morita: Mater. Trans. (2005) vol. 46, pp. 1335-40

49. R.N. Hall, "Segregation of Impurities During the Growth of Germanium and Silicon", J. Phys. Chem., 57 (1953) 836-839

50. Baba et al, "Removal of Boron from Molten Silicon by Argon-Plasma Mixed with Water Vapor", Proceeding of the International Conference on Photovoltaic Solar Energy, Vol. 10th (1991) p.286

51. Yuge et al, " Purification of metallurgical silicon up to solar grade", Solar Energy Materials and Solar Cells 34 (1994) 243-250

52. Yuge et al, "Purification of metallurgical grade silicon up to solar grade", Prg. Photovolt: Res. Appl. (2001) 9, 203-209

53. Tanahashi et al, "Removal of boron from metallurgical-grade silicon by applying CaO-based flux treatment", Yazawa International Symposium: Metallurgical and Materials Processing, Vol.1 (2003) 613-624

54. Tanahashi et al, "Oxidation Removal Behavior of Boron and Local Nonequilibrium Reaction Field in Purification Process of Molten Silicon by The Flux Injection Technique", Sohn International Symposium: Advanced Processing of Metals and Materials, Vol.1 (2006) 173-186

55. Huge et al., “Solar Energy Materials and Solar Cells”, 34 (1994) pp. 243-250

56. J. Safarian and M. Tangstad, “Kinetics and Mechanism of Phosphorus Removal from Silicon in Vacuum Induction Refining”, High Temperature Materials and Processes, issue 6, Vol. 30, Jan 2012

57. T. Ikeda and M. Maeda, “Elimination of Boron in Molten Silicon by Reactive Rotating Plasma Arc Melting”, Materials Transactions, JIM, Vol. 37, No. 5 (1996), pp 983-987

58. K. Suzuki, T. Kumagai and N. Sano, ISIJ International, 32 (1992) 630

59. Tang et al., "Removal of Boron in Silicon by $H_2$-$H_2O$ Gas Mixture", JOM Vol. 64, No. 8, pp. 952-956, Aug 2012

60. Tang et al., " Critical assessment of the impurity diffusivities in solid and liquid silicon", JOM, Vol.61, No. 11, Nov. 2009

61. Jian-Guo Li, "Wetting of Ceramic Materials by Liquid Silicon, Aluminium and Metallic Melts Containing Titanium and Other Reactive Elements: A Review", Ceramics International 20 (1994) 391-412

62. Svyatoslav et al., "Wettability Effect on Bubble Formation at Nozzles in Liquid Aluminum", Materials Transactions, Vol. 44, No. 11 (2003) pp. 2298 to 2302

63. Millot et al., "The surface tension of liquid silicon at high temperature", Materials Science and Engineering: A, Volume 495, Issues 1–2, 2008, P. 8–13

64. G. A. Irons and R. I. L. Guthrie, "Bubbling Behavior in Molten Metals", Canadian Metallurgical Quarterly, Vol. 19, No.4, pp. 381-387, 1981

65. Gnyloskurenko et. al., "Wettability Effect on Bubble Formation at Nozzles in Liquid Aluminum", Materials Transactions, Vol. 44, No. 11 (2003) pp. 2298 to 2302

66. R. Clift, J.R. Grace, "Bubbles, Drops and Particles", Academic Press, 1978